HPCA1 is required for systemic ROS and calcium cell-to-cell signaling and plant acclimation to stress

Yosef Fichman[1], Sara I Zandalinas[2], Scott Peck[3], Sheng Luan[4], Ron Mittler[1,5,*]

[1]Division of Plant Sciences and Technology, College of Agriculture Food and Natural Resources and Interdisciplinary Plant Group, University of Missouri, Columbia, MO 65211, USA.

[2]Department of Agricultural and Environmental Sciences, University Jaume I, Castelló de la Plana, 12071, Spain.

[3]Department of Biochemistry, College of Agriculture Food and Natural Resources and Interdisciplinary Plant Group, University of Missouri, Columbia, MO 65211, USA.

[4]Department of Plant and Microbial Biology, University of California, Berkeley, CA 94720, USA.

[5]Department of Surgery, University of Missouri School of Medicine, Christopher S. Bond Life Sciences Center, University of Missouri, Columbia, MO 65201, USA

Short title: HPCA1 is required for systemic signaling.

***Corresponding author:** Ron Mittler (mittlerr@missouri.edu)

The author(s) responsible for distribution of materials integral to the findings presented in this article in accordance with the policy described in the Instructions for Authors (https://academic.oup.com/plcell/pages/General-Instructions) is Ron Mittler (mittlerr@missouri.edu)

ABSTRACT

Reactive oxygen species (ROS), produced by respiratory burst oxidase homologs (RBOHs) at the apoplast, play a key role in local and systemic cell-to-cell signaling, required for plant acclimation to stress. Here we reveal that the leucine-rich-repeat receptor-like kinase HPCA1 (H_2O_2-induced Ca^{2+} increases 1) acts as a central ROS receptor required for the propagation of cell-to-cell ROS signals, systemic signaling in response to different biotic and abiotic stresses, stress responses at the local tissue, and plant acclimation to stress, following a local treatment of high light stress. We further report that HPCA1 is required for systemic calcium signals, but not systemic membrane depolarization responses, and identify the calcium-permeable channel mechanosensitive ion channel like 3 (MSL3), calcineurin B-like calcium sensor (CBL4), CBL4-interacting protein kinase 26 (CIPK26), and sucrose-non-fermenting-1-related protein kinase 2.6 (Open stomata 1; OST1) as required for the propagation of cell-to-cell ROS signals. In addition, we identify serine residues S343 and S347 of RBOHD (the putative targets of OST1) as playing a key role in cell-to-cell ROS signaling in response to a local application of high light stress. Our findings reveal that HPCA1 plays a key role in mediating and coordinating systemic cell-to-cell ROS and calcium signals required for plant acclimation to stress.

INTRODUCTION

Reactive oxygen species (ROS; *i.e.,* H_2O_2, $O_2^{\cdot-}$, $^1O_2$, and $HO^{\cdot}$) are credited with playing a fundamental role in the evolution of life on Earth impacting processes such as the endosymbiotic event, emergence of multicellularity, and the development of reproduction through sex (Taverne et al., 2018; Hörandl and Speijer, 2018; Gutteridge and Halliwell, 2018; Jabłońska and Tawfik, 2021). Although originally considered to be toxic byproducts of aerobic metabolism, in recent years numerous studies revealed that ROS, such as H_2O_2 and $O_2^{\cdot-}$, are essential for life, acting as key regulators of redox, stress responses, and cell-to-cell signaling (Schieber and Chandel, 2014; Mittler, 2017; Sies and Jones, 2020; Mittler et al., 2022). Examples for the role of ROS in cell-to-cell signaling include the recruitment of macrophages to wound sites and interactions between neurons in animals, communication between microorganisms within a microbiome, and transmission of long-distance cell-to-cell signals in plants (Aguirre and Lambeth, 2010; Razzell et al., 2013; Zheng et al., 2015; Zandalinas et al., 2020a; Zandalinas et al., 2020b; Fichman et al., 2021; Iwashita et al., 2021). In the flowering plant *Arabidopsis thaliana* (Arabidopsis), cell-to-cell ROS signaling plays a pivotal role in local and systemic responses, acclimation, and survival of plants during stress (Mittler et al., 2011; Zhu, 2016; Waszczak et al., 2018; Smirnoff and Arnaud, 2019; Zandalinas et al., 2020a; Zandalinas et al., 2020b; Fichman et al., 2021; Mittler et al., 2022). During this process, ROS production is triggered in cells directly subjected to stress (termed 'local tissue'), and a state of 'activated ROS production', driven by the function of respiratory burst oxidase homologs (RBOHs; the plant equivalents of mammalian NADPH oxidases; NOXs), is propagated from cell-to-cell over long distances, sometime spanning the entire length of the plant (Mittler et al., 2011; Zhu, 2016; Fichman et al., 2019; Zandalinas et al., 2020a; Fichman and Mittler, 2020b; Zandalinas et al., 2020b; Fichman et al., 2021; Mittler et al., 2022). Once the activated ROS production state reaches cells and tissues other than the ones initiating it (*i.e.,* tissues not directly subjected to stress; termed 'systemic tissues'), it activates in them different acclimation mechanisms and enhances the overall resilience of the plant to stress (termed 'systemic acquired acclimation'; SAA; Karpinski et al., 1999; Zandalinas et al., 2020a; Zandalinas et al., 2020b; Fichman et al., 2021). Although the process of cell-to-cell ROS signaling (termed the 'ROS wave') is essential for systemic signaling and SAA to occur, it does not convey specificity to the systemic response and is therefore linked with other, yet unknown, stress-specific systemic signals, as well

as with cell-to-cell calcium and membrane potential signaling processes (Suzuki et al., 2013; Fichman and Mittler, Fichman et al., 2020a, 2021a; Fichman et al., 2021). While RBOHs such as RBOHD and RBOHF were found to produce apoplastic ROS essential for this process (Miller et al., 2009; Fichman et al., 2019; Zandalinas et al., 2020a; Fichman and Mittler, 2020b; Zandalinas et al., 2020b; Fichman et al., 2021; Mittler et al., 2022), the identity of the ROS receptor(s) perceiving the apoplastic ROS signal and enabling the cell-to-cell ROS signaling process to occur is currently unknown.

We recently developed a new method for whole plant live ROS imaging to visualize cell-to-cell ROS signaling in mature plants growing in soil (Fichman et al., 2019; Fichman and Mittler, 2020b). Using this method, we screened over 120 different mutants, potentially involved in ROS and calcium signaling, for the presence or absence of the ROS wave in response to a local treatment of high light (HL) stress (Supplemental Table 1). Among the different mutants we screened were several putative receptors, including different cysteine-rich receptor-like kinases (CRKs) and the leucine-rich-repeat receptor-like kinase (LRR-RLK) HPCA1 ('H_2O_2-induced Ca^{2+} increases 1'; At5g49760; also known as 'cannot respond to DMBQ 1'; CARD1). HPCA1 was recently identified as a receptor for extracellular H_2O_2 (Wu et al., 2020), as well as a sensor for the oxidizing molecule quinone (Laohavisit et al., 2020). Here we reveal that HPCA1 acts as a key ROS receptor required for the accumulation of ROS in stressed tissues, propagation of cell-to-cell ROS signals, systemic signaling in response to different biotic and abiotic stresses, and plant acclimation to stress. We further show that HPCA1 is required for systemic calcium signals (also termed the 'calcium wave'), but not systemic membrane depolarization responses (a type of 'electric wave'), and that systemic calcium signals mediated by HPCA1 require the function of the calcium-permeable channel mechanosensitive ion channel like 3 (MSL3). In addition, we reveal that key components of calcium-dependent signaling cascades, such as the calcineurin B-like calcium sensor (CBL4), the CBL4-interacting protein kinase 26 (CIPK26), and the sucrose-non-fermenting-1-related protein kinase 2.6 (SnRK2.6, also termed 'open stomata 1', OST1), are also involved in this process. We further identify serine residues S343 and S347 of RBOHD (the putative targets of OST1) as playing a key role in cell-to-cell ROS signaling in response to a local application of HL stress. Our findings reveal that HPCA1 plays a key role in the sensing of H_2O_2 produced at the apoplast during cell-to-cell signaling, linking the accumulation of apoplastic H_2O_2 with calcium cascades and the activation of further ROS production by RBOHs; thereby mediating

and coordinating systemic cell-to-cell ROS and calcium signals that are required for plant resilience to stress.

RESULTS

HPCA1 is required for systemic cell-to-cell ROS and calcium signaling during plant responses to HL stress

To study the role of HPCA1 in systemic cell-to-cell ROS signaling, we subjected a single leaf of wild-type (WT) and two independent knockout alleles of HPCA1 (*hpca1-1, hpca1-2*) to a HL stress treatment of 1700 µmol photons $s^{-1}m^{-2}$ for 2 min and used our newly developed whole-plant live ROS imaging method with 2',7'-dichlorodihydrofluorescein diacetate (H_2DCFDA) as a probe (Fichman et al., 2019) to measure the accumulation of ROS in local and systemic leaves over a period of 30 min. High light stress can occur in shaded plants or shaded canopy leaves as a result of sunflecks, or in field grown plants when the sun light is intermittently blocked by clouds (Karpinski et al., 1999; Kromdijk et al., 2016; Slattery et al., 2018). As shown in Figure 1A, mutants deficient in HPCA1 (*hpca1-1, hpca1-2*) did not accumulate ROS in their local or systemic leaves in response to a local application of HL stress (see also Supplemental Movie 1). Because H_2DCFDA detects a broad range of different ROS, we also used Peroxy Orange 1 (PO1; Fichman et al., 2019) instead of H_2DCFDA as a probe, to measure the levels of H_2O_2 that accumulate in local and systemic leaves of WT, *hpca1-1,* and *hpca1-2* plants following a similar HL treatment. As shown in Figure 1B, H_2O_2 accumulated in local and systemic leaves of WT, but not the *hpca1-1* and *hpca1*-2 mutants in response to a local treatment of HL stress. Similar results were also observed in extracts obtained from treated and untreated local and systemic leaves of WT, *hpca1-1,* and *hpca1-2* plants when the levels of H_2O_2 were quantified using the Amplex®-Red method (Figure 1C).

Upon sensing of H_2O_2, HPCA1 was found to trigger the accumulation of calcium in the cytosol (Wu et al., 2020). This process could activate another type of cell-to-cell signaling pathway

termed the 'calcium wave' (dependent on the function of the calcium channels glutamate-like receptor 3.3 and 3.6; GLRs; Evans et al., 2016; Toyota et al., 2018; Shao et al., 2020; Fichman and Mittler, 2021a). To determine whether HPCA1 is also required for systemic cell-to-cell calcium signals, we subjected a single leaf of WT, *hpca1-1,* and *hpca1-2* plants to the same HL stress treatment described above and used Fluo-4-AM as a probe in our live imaging platform (Fichman and Mittler, 2021a) to measure changes in cytosolic calcium levels in local and systemic leaves over a period of 30 min. As shown in Figure 2A, mutants deficient in HPCA1 (*hpca1-1, hpca1-2*) did not display local or systemic changes in cytosolic calcium levels in response to a local application of HL stress (see also Supplemental Movie 1). Interestingly, the HL-induced local and systemic calcium signal observed in WT plants was not transient (Figure 2; Supplemental Movie 1). This finding agrees with our previous findings (Fichman and Mittler 2021a) and the work of Toyota et al., (2018), and corresponds with the elevated levels of local and systemic ROS that persist for about 3-6 hours post a 2- or 10-min HL stress treatment of a local leaf (Devireddy et al., 2020; Fichman et al., 2019).

Systemic cell-to-cell ROS signals were previously found to be dependent on several different calcium-permeable channels including MSL3 (Supplemental Table 1; Fichman et al., 2021). We therefore used the method described above (Figure 2A) to test whether systemic cell-to-cell cytosolic calcium changes are dependent on MSL3. As shown in Figure 2B, in response to a local HL treatment, *msl3-1,* and *msl3-2* mutants did not display local or systemic changes in cytosolic calcium levels. Furthermore, in contrast to WT, the *msl3-1* mutant did not display local or systemic changes in cytosolic calcium levels in response to a local treatment of 1 mM H_2O_2 (Supplemental Figure 1). These finding suggest that MSL3 could function downstream to HPCA1.

Systemic cell-to-cell calcium and ROS signals were previously proposed to be linked with another type of cell-to-cell signaling, termed the 'electric wave' (a rapid depolarization of the plasma membrane, also dependent on the function of GLRs; Mousavi et al., 2013; Nguyen et al., 2018; Farmer et al., 2020; Fichman and Mittler, 2021a). To determine whether HPCA1 is also required for systemic cell-to-cell membrane depolarization signals, we subjected a single leaf of WT, *hpca1-1,* and *hpca1-2* plants to the same HL stress treatment described above and used $DiBAC_4(3)$ as a probe in our live imaging platform (Fichman and Mittler, 2021a) to measure these changes in local and systemic leaves over a period of 30 min. Interestingly, while the systemic cell-to-cell calcium and ROS signals were suppressed in the *hpca1* mutants (Figures 1, 2;

Supplemental Movie 1), the rapid local and systemic membrane depolarization signal was not (Figure 3; Supplemental Movie 1). In contrast to the *hpca1* mutants, and in agreement with our previous characterization of the *glr3.3glr3.6* double mutant (Fichman and Mittler, 2021a), cell-to-cell membrane depolarization signals were suppressed in the *glr3.3glr3.6* double mutant in response to a local application of HL stress (Figure 3).

The findings presented in Figures 1-3 suggest that HPCA1 is required for local accumulation of H_2O_2 during light stress, as well as for the activation of the calcium and ROS (but not electric) waves in response to a local treatment of HL stress.

HPCA1 is required for local and systemic expression of different acclimation transcripts as well as for local and systemic plant acclimation to HL stress

Suppression of systemic cell-to-cell ROS and/or calcium signals (Figures 1, 2) could prevent plants from acclimating to stress. To test whether HPCA1 mutants are deficient in plant acclimation, we measured the local and systemic expression of several transcripts associated with plant acclimation to excess light stress 30 min following the application of HL (1700 µmol photons $s^{-1}m^{-2}$) stress for 2 min to a local leaf of WT and *hpca1-1* plants. As shown in Figure 4A, the expression of *MYELOBLASTOSIS DOMAIN PROTEIN 30 (MYB30), ZINC FINGER OF ARABIDOPSIS THALIANA 10 and 12 (ZAT10 and ZAT12)*, *ASCORBATE PEROXIDASE 2 (APX2)*, and *ZINC FINGER HOMEODOMAIN* 5 (ZHD5), was upregulated in local and systemic leaves of WT plants in response to the local HL stress treatment. In contrast, except for APX2 that was upregulated in local leaves of *hpca1-1* plants, the expression of all transcripts was suppressed in local and systemic leaves of *hpca1-1* plants in response the local HL stress treatment (Figure 4A).

The lack of systemic ROS and calcium cell-to-cell signals (Figures 1, 2), as well as systemic expression of *MYB30*, *ZAT10*, *ZAT12*, *APX2* and *ZHD5* (Figure 4A), could suggest that HPCA1 is required for systemic acclimation of plants to HL stress. To test this possibility, we measured the acclimation (*i.e.,* reduced tissue damage following exposure to light stress) of mature WT and *hpca1-1* plants to a prolonged HL stress treatment following a short pretreatment with HL stress and an incubation period. As shown in Figure 4B, pretreatment of WT plants with 10 min of HL stress, followed by an incubation of 50 min under controlled growth conditions, protected

local and systemic leaves of plants from a subsequent exposure to 45 min of HL stress (*i.e.,* prevented leaf injury as measured by electrolyte leakage, compared to plants that were subjected to the 45 min HL treatment without a 10 min pretreatment with excess white or red light). In contrast, pretreatment of *hpca1-1* plants with a short HL stress failed to induce local or systemic leaf acclimation to a subsequent prolonged HL stress that resulted in a significant increase in electrolyte leakage from cells (Figure 4B).

The findings presented in Figure 4 suggest that although the HL stress is sensed at the local leaves of the *hpca1* mutants (evident by increased expression of *APX2*), these mutants are deficient in many other aspects of local and systemic plant responses and acclimation to HL stress.

HPCA1 is required for the propagation of the HL-induced systemic ROS signal

Systemic cell-to-cell ROS signaling is driven by two different pathways, one that controls its initiation at the local tissue, and one that controls its propagation-, amplification-, and acclimation-promoting functions, in local and systemic tissues (Fichman et al., 2021; Mittler et al., 2022). In addition to these pathways, are other systemic signaling pathways such as the calcium, membrane potential (electric), and stress-specific signals (Suzuki et al., 2013; Fichman and Mittler, 2021a; Fichman et al., 2020a, 2021a; Fichman et al., 2021). The relationship between some of these systemic signals can be distinguished in plants by grafting experiments between WT plants and different mutants (Suzuki et al., 2013; Fichman et al., 2021). Using such grafting experiments, we found that HPCA1 is required for the propagation but not initiation of the HL-induced systemic ROS signal (Figure 5). Thus, while the *hpca1-1* mutant was deficient in ROS wave propagation through the scion (systemic tissue), following the activation of the ROS wave at the WT stock (that includes the local tissue), it could transmit other systemic signals that are not the ROS wave through the (local) stock tissue to a WT scion triggering in it the ROS wave (Figure 5A-5C). In contrast, the *rbohD* mutant was deficient in both systemic signal initiation and propagation (Figure 5D; Supplemental Figure 2; Fichman et al., 2021), while the *rbohF* mutant was similar to *hpca1-1* mutant and was only deficient in systemic ROS wave propagation (Figure 5E; Supplemental Figure 2).

HPCA1 is therefore required for the propagation of the systemic cell-to-cell ROS signal (Figure 5A-5C), as well as for its transcript accumulation- and acclimation-driven functions in systemic tissues (Figure 4). HPCA1 is however not required for some of the other systemic signals that can propagate through a stock that lacks HPCA1 (*hpca1*) into a WT scion and trigger in it the ROS wave. Because HPCA1 is not required for the membrane potential signal to propagate in response to a local HL stress treatment (Figure 3), but RBOHD is (Suzuki et al., 2013; Fichman and Mittler, 2021a), an electric wave produced by the local HL stress in the *hpca1* stock could be one of the other systemic signals that propagates through this stock into the WT scion triggering in it the ROS wave.

HPCA1 is required for systemic cell-to-cell ROS signaling in response to a local bacterial infection or salt stress, but not wounding

The findings that HPCA1 is required for the propagation of the ROS wave (Figure 5A-5C), that plays a key role in plant responses to many different abiotic stresses (Zhu, 2016; Fichman et al., 2019; Zandalinas et al., 2020a; Fichman and Mittler, 2020b; Zandalinas et al., 2020b; Fichman et al., 2021; Mittler et al., 2022), could suggest that HPCA1 is involved in plant responses to a broad range of stresses. To test the involvement of HPCA1 in local and systemic ROS responses to other stresses, we treated a local leaf of WT or *hpca1-1* plants with a bacterial pathogen (*P. syringae* DC 3000; 10^6 CFU/ml; Fichman et al., 2019), salt stress (100 mM NaCl), or wounding (Simultaneously piercing with 20 dresser pines; Fichman et al., 2019), and measured local and systemic accumulation of ROS (untreated, or mock buffer treatment in the absence of the pathogen or salt were used as controls). As shown in Figure 6, while all treatments caused the accumulation of ROS in local and systemic leaves of WT plants, *hpca1-1* plants did not respond to the bacterial pathogen or salt stress treatments (Figure 6A, 6B). In response to a local treatment of wounding, *hpca1-1* mutants did however display a local and systemic cell-to-cell ROS signaling response that was indistinguishable from that of WT (Figure 6C). These findings suggest that cell-to-cell ROS signals could be mediated in plants by more than one type of ROS receptor. Systemic cell-to-cell ROS signaling pathways, triggered by HL stress, bacterial infection, or salinity treatments (Figures 1, 6A, 6B) and mediated by HPCA1, could therefore be distinguished from those activated by

wounding (Figure 6C) and potentially mediated by a yet unknown ROS receptor(s). In a previous study, treatment of *hpca1* seedlings with 100 mM NaCl triggered changes in calcium levels (Wu et al., 2020). In agreement with these studies, we also found that salt stress (100 mM NaCl) triggers a calcium wave in the *hpca1-1* mutant (Supplemental Figure 3); but not a ROS wave (Figure 6B). Salt stress (100 mM NaCl) was also found to triggers a calcium wave in *msl3-1* mutant (Supplemental Figure 3). Taken together, these findings suggest that the calcium wave could be mediated via different molecular mechanisms during HL and salt stresses [*i.e.,* MSL3 during HL stress, as opposed to two-pore channel 1 (TPC1) during salt stress; Figures 2, 6; Evans et al., 2016]. Further studies are required to address the coupling of the ROS and calcium waves during salt, HL, and other biotic and abiotic stresses.

HPCA1-dependent cell-to-cell ROS signaling requires the central calcium signaling regulators CBL4, CIPK26, and OST1

The increase in calcium levels resulting from HPCA1 activation during local and systemic responses to HL stress (Figure 2) could cause the activation of calcium-dependent protein kinase cascades and trigger ROS production by RBOHs (Luan and Wang, 2021; Mittler et al., 2022). Our mutant screen (Supplemental Table 1) identified three proteins potentially involved in such cascades (CBL4, CIPK26, and OST1). As shown in Figure 7A, similar to the *hpca1-1* mutant (Figure 1), *cbl4-1*, *cipk26-2*, and *ost1-2* mutants were deficient in mediating the systemic cell-to-cell ROS signal in response to a 2 min local treatment of HL stress. In addition, and also similar to the *hpca1-1* mutant (Figure 4B), *cbl4-1*, *cipk26-2*, and *ost1-2* mutants were unable to acclimate to HL stress following a pretreatment with a short period of HL stress (Figure 7B).

To test whether CBL4, CIPK26, and OST1 are required for the initiation or propagation of the systemic cell-to-cell ROS signal, we conducted grafting experiments between these mutants and WT plants (Figure 8; similar to the analysis described in Figure 5). These studies revealed that like HPCA1 (Figure 5), CBL4, CIPK26, and OST1 are all required for the propagation of the systemic cell-to-cell ROS signal. Thus, while the *cbl4-1*, *cipk26-2*, and *ost1-2* mutants were deficient in ROS wave propagation through the scion (systemic tissue), following the activation of the ROS wave at the WT stock (that includes the local tissue), they could transmit other HL-

induced systemic signals that are not the ROS wave through the (local) stock tissue to a WT scion and trigger in it the ROS wave (Figure 8). The findings that key components of a calcium-dependent signaling cascade (*i.e.,* CBL4, CIPK26, and OST1) are required for the propagation of the cell-to-cell ROS signal reveal that enhanced levels of calcium alone (Figure 2) are not sufficient to trigger the ROS wave by directly interacting with the calcium-binding domains of RBOHD (Ogasawara et al., 2008). Rather, an amplification cascade of the signal is needed. The results presented in Figures 3, 5, 7, and 8 also suggest that HPCA1, CBL4, CIPK26 and OST1 are not required for the propagation of other HL-induced systemic signals such as the electric wave that are initiated in the local tissue (stock; Figure 3).

The same amino acid residue required for RBOHD activation by OST1 is also required for RBOHD activation during systemic cell-to-cell ROS signaling

The sensing of high cytosolic calcium levels by CBL4 was shown to activate CIPK26, and CIPK26 was shown to phosphorylate and activate RBOHF (Drerup et al., 2013). CIPK26 was also shown to interact with OST1 (Mogami et al., 2015). OST1, in turn, is thought to phosphorylate RBOHD on serine 347 and activate it (Wang et al., 2020). OST1 was also shown to phosphorylate and activate RBOHF (Sirichandra et al., 2009). Because RBOHD plays such a canonical role in the initiation and propagation of the systemic cell-to-cell ROS signal (Figure 5; Supplemental Figure 2; Zandalinas et al., 2020a; Zandalinas et al., 2020b; Fichman et al., 2021), we tested whether deleting its N-terminal regulatory domain (RD; amino acids 1 to 347), or mutating serine 347 to alanine (the target of OST1 phosphorylation; Wang et al., 2020), will inhibit the systemic cell-to-cell ROS signal in response to HL stress. For this purpose, we expressed the WT *RbohD* gene (RbohD genomic; Figure 9), or the *RbohD* cDNA (RbohD cDNA; Figure 9), under the control of the *RbohD* promoter in *rbohD* mutants. In addition, we expressed the *RbohD* cDNA without the RD (RbohD w/o RD; Figure 9), or the RbohD gene with point mutations (Serine to Alanine) in positions 22 and 26 (RbohD S22-26A; Figure 9), or 22, 26, 343 and 347 (RbohD S22-26,343-347A; Figure 9) in the *rbohD* mutant (Nühse et al., 2007; Zandalinas et al., 2020b). Phosphorylation of RBOHD on S343/S347, as well as on S22/S26 was previously associated with the RBOHD- and ROS-dependent innate immune response of Arabidopsis (with S343/S347

playing a key role in this response; Nühse et al., 2007), and the WT *RbohD* gene expressed under the control of the *RbohD* promoter was shown to complement local and systemic ROS production in response to HL stress in the *rbohD* mutant (Zandalinas et al., 2020b). Once we confirmed that all transgenic complementation assays were homozygous and expressing a single copy of the transgene, we subjected a single leaf of WT, *rbohD*, *rbohD*RbohD genomic, *rbohD*RbohD cDNA, *rbohD*RbohD w/o RD, *rbohD*RbohD S22-26A, and *rbohD*RbohD S22-26,343-347A to a 2 min of HL stress treatment (as described for Figure 1) and measured ROS accumulation in local and systemic leaves. As shown in Figure 9A and 9B, complementation of the *rbohD* mutant with the WT *RbohD*, WT *RbohD* cDNA, or *RbohD* S22-26A restored the systemic cell-to-cell ROS response. In contrast, complementation of the *rbohD* mutant with the *RbohD* w/o RD, or the *RbohD* S22-26,343-347A failed to restore the systemic ROS signal.

To study the expression of the key HL acclimation response gene *Zat12* in *rbohD* mutants transformed with the different constructs, we conducted the same analysis described above, however instead of the *rbohD* mutant we used the double homozygous line expressing the *Zat12::luciferase* reporter in the *rbohD* background (developed as described in Miller et al., 2009; Zandalinas et al., 2020b) for the complementation study. As shown in Figure 9C, expression of the *Zat12* gene (measured by luciferase activity; Miller et al., 2009; Zandalinas et al., 2020b) was significantly elevated only in *rbohDZat12::luciferase* lines complemented with the WT *RbohD*, WT *RbohD* cDNA, or *RbohD* S22-26A (as well as in WT plants transformed with the *Zat12::luciferase* reporter). In contrast, *Zat12* expression was not complemented in *rbohDZat12::luciferase* lines by expression of the *RbohD* w/o RD or the *RbohD* S22-26,343-347A constructs. These findings agreed with the measurements of local and systemic ROS shown for the different complemented *rbohD* lines in panels A and B.

To study systemic acclimation to HL stress we also subjected the *rbohD* complemented lines (Figure 9A, 9B) to the same HL SAA assay shown in Figures 4B and 7B. As shown in Figure 9D, complementation of the *rbohD* mutant with the WT *RbohD*, WT *RbohD* cDNA, or *RbohD* S22-26A restored systemic HL acclimation to the *rbohD* mutant, while complementation of the *rbohD* mutant with the *RbohD* w/o RD or the *RbohD* S22-26,343-347A construct did not.

Taken together, the analyses shown in Figure 9 suggest that complementation of *rbohD* with the wild type *RbohD* gene, cDNA, or *RbohD* gene with mutations in S22 and S26 (Nühse et al., 2007; Zandalinas et al., 2020b), restored HL-induced systemic cell-to-cell ROS signaling

(Figure 9A), systemic *Zat12* gene expression (Figure 9B), and systemic acclimation to HL stress (Figure 9C). By contrast, complementation of *rbohD* with the *RbohD* cDNA that lacks the RD, or the *RbohD* gene that contains point mutations in S22, S26, S343 and S347 (Nühse et al., 2007), did not restore the ROS wave, systemic *Zat12* expression, or systemic acclimation to HL (Figure 9). These findings point to residues S343 and S347 (the target of OST1; Wang et al., 2020) as playing a key role in cell-to-cell ROS signaling.

DISCUSSION

The ability of plants to mobilize a signal from a small group of cells subjected to stress to the entire plant, *i.e.,* systemic signaling, plays a pivotal role in plant acclimation to, and/or defense against, many different abiotic and biotic stresses (Mittler et al., 2011; Zhu, 2016; Waszczak et al., 2018; Smirnoff and Arnaud, 2019; Farmer et al., 2020; Johns et al., 2021; Mittler et al., 2022). Among the different signal transduction mechanisms that mediate systemic responses in plants is a rapid cell-to-cell signaling process that involves membrane depolarization, cytosolic calcium alterations, and ROS accumulation (Figures 1-3, Supplemental Movie 1; Mittler et al., 2011; Farmer et al., 2020; Fichman and Mittler, 2020a; Shao et al., 2020; Johns et al., 2021; Mittler et al., 2022). Previous studies identified RBOHD, RBOHF, and GLR3.3GLR3.6 as key players in this cell-to-cell response (Miller et al., 2009; Mousavi et al., 2013; Toyota et al., 2018; Shao et al., 2020; Zandalinas et al., 2020b). While RBOHs were shown to mediate ROS production required for cell-to-cell signaling and plant acclimation (Miller et al., 2009; Fichman et al., 2019), GLRs were shown to mediate membrane depolarization and alterations in calcium levels (that could potentially drive ROS production; Mousavi et al., 2013; Evans et al., 2016; Toyota et al., 2018; Nguyen et al., 2018; Shao et al., 2020; Fichman and Mittler, 2021a). Prior studies have also suggested that the function of RBOHs and GLRs is interlinked (*e.g.,* Fichman and Mittler, 2020a; Fichman and Mittler, 2021a). Nevertheless, how changes in ROS levels at the apoplast (produced by RBOHs) are translated into changes in cytosolic calcium during cell-to-cell ROS signaling remains unknown. Here we show that HPCA1 plays a canonical role in systemic cell-to-cell signaling in plants, triggering cytosolic calcium accumulation upon sensing of apoplastic ROS/H_2O_2 (Figures

1, 2A, Supplemental Movie 1). The altered calcium levels, potentially driven by MSL3 (Figure 2B; Supplemental Figure 1), could then activate a downstream pathway that requires CBL4, CIPK26, and OST1 and trigger further ROS production (Figures 7-9). HPCA1 may therefore represent a highly important and missing puzzle piece that links changes in apoplastic ROS levels driven by RBOH function with changes in cytosolic calcium levels driven by different calcium-permeable channels such as MSL3 (Figure 10). The finding that HPCA1 is required for systemic ROS and calcium cell-to-cell signaling (Figures 1, 2A), the expression of many acclimation transcripts in local and systemic tissues (Figure 4A), as well as plant acclimation (Figure 4B), provides strong support to this proposed role of HPCA1. Because some of the interactions between CBL4, CIPK26, OST1, and RBOHD/F were identified *in vitro* (*e.g.,* Wang et al., 2020), further studies would be needed to dissect the calcium signaling cascades that function downstream of HPCA1. Additional studies are also required to identify the mode of HPCA1 activation during this process (Wu et al., 2020).

Interestingly, in our hands, HPCA1 appears not to be needed for the mediation of systemic membrane potential changes (Figure 3; Supplemental Movie 1). In this respect it should also be noted that our grafting experiments (Figure 5) revealed that the mobilization of other HL-induced systemic signals, that are not the ROS wave, through a scion made from *hpca1-1* (without the accumulation of detectable ROS levels) could lead to the activation of the ROS cell-to-cell signal in the WT scion (Figure 5). Taken together, these findings suggest that a cell-to-cell membrane potential signal could mediate the HL-induced systemic signal in the *hpca1* mutant even in the absence of the ROS and/or calcium cell-to-cell signals (Figures 1-3, 5; Supplemental Movie). HPCA1 is however required in local and systemic plant tissues to enhance transcript expression and acquire a heightened state of acclimation; Figure 4). The notion that the electric wave could be playing a role in mediating systemic signaling to a local HL stress is also supported by the pace of the different systemic signals detected in our study (Figure 1-3; Supplemental Movie 1). The systemic change in membrane potential (a type of electric wave) is the fastest, followed by a change in cell-to-cell cytosolic calcium levels, that are followed by changes in cell-to-cell ROS levels (Figures 1-3; Supplemental Movie 1). These observations could suggest that an electric wave (that is GLR-dependent, at least for its initiation; Mousavi et al., 2013; Nguyen et al., 2018; Fichman and Mittler, 2021a) is the first to reach all cells. The changes in membrane potential it brings with it may prime, alter, or activate different channels and other signaling mechanisms.

These could then trigger a calcium wave [that could be dependent on GLRs, MSLs, TPC1, and/or cyclic nucleotide–gated ion channels (CNGCs); Evans et al., 2016; Toyota et al., 2018; Shao et al., 2020; Fichman et al., 2021; Dickinson et al., 2022)], that in turn activate ROS production via CBL4-, CIPK26- and/or OST1-mediated RBOH activation (Figures 7-10). Although calcium changes are imaged in our system before ROS changes (Figures 1-3; Supplemental Movie 1), the new player in this pathway, introduced by this work, *i.e.,* HPCA1, appears to be required for integrating the cell-to-cell calcium and ROS signals, providing a mechanistic understanding to how changes in apoplastic ROS levels are linked to changes in cytosolic calcium levels (Figure 10; Supplemental Movie 1). The possible role of electric signals in activating cell-to-cell ROS signaling is also supported by a recent study showing that aboveground plant-to-plant transmission of electric signals (via two physically touching leaves) can trigger the cell-to-cell ROS signal in a receiving plant, and that this communication process is dependent on GLRs, RBOHs and MSLs (Szechynska-Hebda et al., 2022). In addition, as shown in Figure 5E and Supplemental Figure 2, as well as reported previously (Fichman et al., 2021), a HL-induced systemic signal cannot propagate through a stock made from the *rbohD* mutant and trigger the ROS wave in a WT scion. In this respect it should be noted that RBOHD is required for the propagation of the electric wave in response to a local application of HL stress (Suzuki et al., 2013; Fichman and Mittler, 2021a). The electric wave that propagates independently of HPCA1 (Figure 3) could therefore trigger the ROS and calcium waves that are dependent on each other, as well as on HPCA1 (Figures 1-3, 5, 7; Supplemental Figure 2; Supplemental Movie 1), providing a possible hierarchy for systemic signaling in response to a local treatment of HL stress.

Interestingly, although HPCA1 was found to be required for systemic cell-to-cell ROS responses to local HL, salt, or pathogen treatments (Figures 1, 6), it was not required for cell-to-cell ROS signaling in response to wounding (Figure 6). This finding could suggest that different receptors for apoplastic ROS are involved in mediating systemic cell-to-cell signaling in response to different stresses. Alternatively, the sensing of changes in apoplastic ROS levels may not play a key role in systemic cell-to-cell signaling in response to wounding. In this respect it should be noted that in addition to being sensed at the plasma membrane by HPCA1, ROS (H_2O_2) can also enter the cytosol from the apoplast through aquaporins (Rodrigues et al., 2017; Fichman et al., 2021; Figure 10). A recent study has shown for example that in the aquaporin mutant plasma membrane intrinsic protein 2;1 (*pip2;1*), the cell-to-cell ROS signal triggered by HL stress is

458 abolished (Fichman et al., 2021; Mittler et al., 2022). ROS could also move from cell-to-cell via
459 plasmodesmata that open in an RBOHD-dependent manner during the progression of the cell-to-
460 cell signal (Fichman et al., 2021). We previously showed that systemic cell-to-cell ROS responses
461 are only suppressed in the *glr3.3glr3.6* double mutant in response to HL stress but are completely
462 abolished in response to wounding (Fichman et al., 2021; Fichman and Mittler, 2021a). Systemic
463 responses to wounding may therefore be more dependent on GLRs and other apoplastic and/or
464 cytosolic ROS sensors, compared to systemic responses to HL stress (Mittler et al., 2022; Mousavi
465 et al., 2013; Toyota et al., 2018; Shao et al., 2020; Fichman and Mittler, 2021a). In addition, they
466 could be mediated through different cell layers that use different mechanisms for systemic cell-to-
467 cell ROS signaling (*i.e.,* mesophyll compared to vascular; Zandalinas et al., 2020b). Further studies
468 are needed to address the relationships between different types of stress and apoplastic sensing of
469 ROS via HPCA1, cytosolic sensing of ROS following their entry into the cell via aquaporins, and
470 the transfer of ROS from cell-to-cell via plasmodesmata (Figure 10; Fichman et al., 2021).
471 In addition to its role in propagating the ROS wave (Figure 5), HPCA1 is also playing a
472 role in ROS and calcium accumulation at the local tissue that is directly exposed to the HL stress
473 (Figures 1, 2). Moreover, HPCA1 is required for the expression of several stress-response
474 transcripts at the local tissue (but not *APX2*) and for acclimation of the local tissue to HL stress
475 (Figure 4). These findings suggest that HPCA1 plays a role in the sensing of the stress at the local
476 tissue. We previously showed that the activation of RBOHD by HL stress at the local tissue
477 requires Phytochrome B (phyB; Devireddy et al., 2020; Fichman et al., 2022; Figure 10). Light
478 stress, that is sensed by phyB or chloroplasts could therefore trigger RBOHD at the local tissue,
479 and the ROS produced by RBOHD could be sensed by HPCA1 leading to further activation of
480 RBOHD in a positive feedback loop that is required for ROS accumulation, defense mechanism
481 activation, and acclimation to HL stress at the local tissue (Figures 1, 4, 10; Mittler et al., 2022).
482 An overall view of rapid cell-to-cell ROS and calcium signaling emerges from our study.
483 In this view each cell in the cell-to-cell ROS signaling pathway senses the ROS generated by the
484 cell preceding it via HPCA1, activates a calcium-dependent signal transduction pathway
485 (involving CBL4, CIPK26 and OST1), and triggers ROS production by RBOHD and RBOHF
486 (Figure 10). The activation of ROS production by that cell is then sensed by the cell following it
487 in the chain, via its own HPCA1, and the process is repeated forming a positive amplification loop
488 that drives the ROS signal from cell-to-cell until all cells in the plant turn their ROS production

state to 'activated'. While the initiation of the cell-to-cell ROS signal is primarily dependent on RBOHD (Miller et al., 2009; Fichman et al., 2019), its propagation is dependent on HPCA1, RBOHD and RBOHF (Figure 5), that together could amplify the ROS signal (Figure 10). CIPK26 can activate RBOHF and OST1 (Drerup et al., 2013; Mogami et al., 2015), while OST1 can activate RBOHD and RBOHF (Sirichandra et al., 2009; Wang et al., 2020; Figures 7-10). Activation of HPCA1 could also cause the opening of aquaporins such as PIP2;1 (Rodrigues et al., 2017; Smirnoff and Arnaud, 2019; Maurel et al., 2021; Mittler et al., 2022) and facilitate the transfer of RBOH-generated ROS into cells. The enhanced production of apoplastic ROS by each cell could therefore alter the ROS and redox state of the cytosol (Fichman and Mittler, 2021b), in an aquaporin- and plasmodesmata-dependent manner (Fichman et al., 2021), and activate multiple transcriptional regulators such as MYB30 and ZAT12 (Figure 4; Fichman et al., 2020c; Mittler et al., 2022), causing all cells 'excited' or 'activated' by the cell-to-cell ROS signal to acquire a heightened state of tolerance to the stress and become acclimated (Figures 4, 7, 9, 10; Zandalinas et al., 2020a; Zandalinas et al., 2020b; Fichman et al., 2021; Fichman and Mittler, 2021b; Mittler et al., 2022). Cell-to-cell ROS signaling therefore plays a key role in plant acclimation to stress, and HPCA1 is a key component of this pathway enabling ROS sensing and continued signal propagation (Figure 10).

METHODS

Plant material, growth conditions and generation of transgenic plants

Arabidopsis thaliana Col-0 wild type plants, homozygous knockout lines (Alonso et al., 2003) of *hpca1* (AT5G49760; CS923304), *cbl4* (AT5G24270; CS859749; Yang et al., 2019), *cipk26* (AT5G21326; SALK_074944C; Lyzenga et al., 2013), *ost1* (AT4G33950; SALK_020604), *msl3* (AT1G58200; SALK_201695C; CS69719), *rbohD* (AT5G47910; CS68747; Torres et al., 2002), and *rbohF* (AT1G64060; CS68748; Torres et al., 2002), as well as native promoter complementation lines of *rbohD* with full-length genomic sequence of *RBOHD*, *RBOHD* S22-

519 26A, *RBOHD* S22-26-343-347A; Nühse et al., 2007), cDNA sequence of *RBOHD* (Zandalinas et
520 al., 2020b) and cDNA sequence of *RBOHD* without its regulatory domain (ΔM1-S347; generated
521 as described below) were used for the main figures (additional mutants are described in
522 Supplemental Table 1). Plants were grown in peat pellets (Jiffy International, Kristiansand,
523 Norway) under controlled conditions of 10hr/14hr light/dark regime, 50 µmol photons s^{-1} m^{-2} and
524 21°C for 4 weeks (Zandalinas et al., 2020a; Zandalinas et al., 2020b; Fichman et al., 2021). For
525 constructing RBOHD without the regulatory domain (ΔM1- S347), a DNA fragment lacking the
526 *RbohD* regulatory domain (from amino acid 348 to 921) was amplified by PCR from cDNA
527 template (using specific primers:
528 5'-GAGACTCGAGATGCAGAAGCTTAGACCGGCAAA-3' and
529 5'-TCTCGAGCTCCTAGAAGTTCTCTTTGTGGAAGT-3'), isolated and sequenced. The
530 resulting *RbohD* sequence without its regulatory domain was cloned into pCAMBIA2301 vectors
531 (Marker Gene Technologies, Eugene, OR, USA) downstream of the native *RbohD* promoter
532 (Nühse et al., 2007; Zandalinas et al., 2020b) replacing the full-length cDNA sequence of *RbohD*
533 (using XhoI and SacI). *Agrobacterium tumefaciens* GV3101 (Koncz and Schell, 1986) was
534 transformed with the binary plasmid and transgenic Arabidopsis plants were generated using floral
535 dipping (Clough and Bent, 1998). Transformed seedlings were selected on 0.5X Murashige and
536 Skoog media plates (Caisson Labs, Smithfield, UT, USA) supplemented with 50 µg ml^{-1}
537 Kanamycin (Gold Bio, St. Louis, MO, USA) for three generations. Transgenic double homozygous
538 pZat12::Luc *rbohD* plants (Miller et al., 2009; Zandalinas et al., 2020b) were also complemented
539 with the different *RbohD* constructs (*i.e.,* full-length genomic sequence of *RbohD*, *RbohD* S22-
540 26A, *RbohD* S22-26-343-347A, cDNA sequence of *RbohD*, and *RbohD* ΔM1-S347) as described
541 above.
542
543
544 **Grafting**
545
546 Grafting was performed as previously described (Fichman et al., 2021). Briefly, Arabidopsis plants
547 (wild-type and different mutants) were germinated on 0.5X Murashige and Skoog media plates
548 (Caisson Labs, Smithfield, UT, USA). An incision was made in seven-day-old stock seedlings to
549 insert a scion into the cut while keeping the rosette of the stock plant intact. Plants were grown for

five days in growth chamber at 20°C under constant light. Surviving grafted plants were transplanted to peat pellets and grown as described above for 5 days before light stress treatment (applied to a single leaf of the stock). For each knockout line, four combinations were constructed and tested: wild-type (WT) as the scion and the stock, the mutant line as the scion and the stock, mutant scion on WT stock, and WT scion on a mutant stock. Grafting was repeated 40 times for each combination of each line with approximately 40% success rate.

Stress application, imaging of ROS, calcium and membrane potential, and H_2O_2 quantification

As previously described (Fichman et al., 2019; Zandalinas et al., 2020b; Fichman and Mittler, 2021a; Supplemental Figure 4), plants were fumigated for 30 min with 50 µM H_2DCFDA (Millipore-Sigma, St. Louis, MO, USA) for ROS imaging (Fichman et al., 2019; Zandalinas et al., 2020b), 4.5 µM Fluo-4-AM (Becton, Dickinson and Company, Franklin Lakes, NJ, USA) for calcium imaging (Fichman and Mittler, 2021a), 20 µM $DiBAC_4(3)$ (Biotium, Fermont, CA, USA) for membrane potential imaging (Fichman and Mittler, 2021a), or 100 µM Peroxy Orange 1 (PO1; Millipore-Sigma, St. Louis, MO, USA) for H_2O_2 imaging (Fichman et al., 2019), using a nebulizer (Punasi Direct, Hong Kong, China) in a glass container. Following fumigation, different stresses were applied as described in (Fichman et al., 2019; Zandalinas et al., 2020b; Fichman and Mittler, 2021a). Briefly, plants were subjected to HL stress by illuminating a single leaf with 1700 µmol photons $s^{-1}m^{-2}$ using a ColdVision fiber optic LED light source (Schott, Southbridge, MA, USA; Fichman et al., 2019; Zandalinas et al., 2020b); pathogen infection was performed by dipping a single leaf in a solution containing DCF and 10^6 CFU of *P. syringae* DC 3000 or the same solution without the bacteria (mock; Fichman et al., 2019); for wounding, a single leaf was pierced simultaneously by 20 dresser pines (Fichman et al., 2019; Fichman and Mittler, 2021a); for salt stress, a single leaf was dipped in 100 mM NaCl, 50 mM phosphate buffer, pH 7.4, with 50 µM H_2DCFDA for 30 seconds (the same solution without NaCl was used for mock control); for H_2O_2 treatment, a single leaf was dipped in 1 mM H_2O_2, 50 mM phosphate buffer, pH 7.4, with 50 µM H_2DCFDA for 30 seconds (the same solution without H_2O_2 was used for mock control). Fluorescence images were acquired using IVIS Lumina S5 (PerkinElmer, Waltham, MA, USA)

for 30 min. ROS, H_2O_2, and calcium accumulation, as well as membrane depolarization were analyzed using Living Image 4.7.2 software (PerkinElmer, Waltham, MA, USA) using the math tools (Fichman et al., 2019; Zandalinas et al., 2020b; Fichman and Mittler, 2021a). Time course images were generated and radiant efficiency of regions of interest (ROI) were calculated. Each data set includes standard error of 8-12 technical repeats. Please note that due to the high sensitivity of this method, background ROS levels are occasionally detected in vascular and meristematic tissues of control untreated plants (Fichman et al., 2019).

Hydrogen peroxide quantification was performed with Amplex®-Red (10-Acetyl-3,7-dihydroxyphenoxazine; ADHP; Thermo Fisher Scientific, Waltham, MA, USA). Local and systemic leaves from the different treatments were flash frozen in liquid nitrogen, ground to fine powder, resuspended in 50 µl 0.1M trichloroacetic acid (TCA; Thermo Fisher Scientific, Waltham, MA, USA), and centrifuged for 15 min at 12,000 g, 4°C. The supernatant was buffered with 1 M phosphate buffer pH 7.4, and the pellet was dried and used for dry weight calculation. H_2O_2 quantification at the supernatant was performed according to the MyQubit-Amplex®-Red Peroxide Assay manual (Thermo Fisher Scientific, Waltham, MA, USA), using a calibration curve of H_2O_2 (Thermo Fisher Scientific, Waltham, MA, USA). In short, 100 µl of the working solution (100 µM ADHP, 0.02 U horseradish peroxide in reaction buffer) was mixed with 100 µl of the sample. After 30 min of incubation in dark, 20 µl from the reaction was diluted in 180 µl of reaction buffer and fluorescence was measured with a Qubit 4 (Thermo Fisher Scientific, Waltham, MA, USA), using the peroxide protocol. Concentration values were normalized to dry weight of each sample.

Systemic acquired acclimation and electrolyte leakage assays

Local and systemic acquired acclimation to HL stress were measured by subjecting a local leaf to light stress (1700 µmol photons $s^{-1}m^{-2}$) for 0 or 10 min, incubating the plant under controlled conditions for 50 min, and then exposing the same leaf (local) or a younger leaf (systemic) to HL stress (1700 µmol photons $s^{-1}m^{-2}$) for 45 min (Zandalinas et al., 2020b; Fichman et al., 2021). Electrolyte leakage was measured by immersing the sampled (treated, untreated, local, or systemic) leaf in distilled water for 1 hr and measuring the conductivity of the water using Oakton CON 700 conductivity meter (Thermo Fisher Scientific, Vernon Hills, IL, USA). Samples were

then boiled with the water, cooled down to room temperature and measured again for conductivity (total leakage). Electrolyte leakage was calculated as percentage of the conductivity before heating the samples over that of the boiled samples and compared between plants treated for 10 min on local leaf (pretreated) or treated for 0 min on their local leaf (non-pretreated). Experiments consisted of 5 repeats for each condition in each line. Standard error was calculated using Microsoft Excel; one-way ANOVA (confidence interval = 0.05) and Tukey honestly significant difference (HSD) were performed with IBM SPSS 25.

Transcript expression

Transcript expression in response to HL stress in local and systemic leaves was measured using 4-week-old wild type and *hpca1-1* plants following the application of HL to a single leaf for 2 min (Fichman and Mittler, 2021a; Fichman et al., 2021). Exposed leaf (local) and unexposed fully developed younger leaf (systemic) were collected for RNA extraction at 0- and 30-min. RNA was extracted using Plant RNeasy kit (Qiagen, Hilden, Germany) according to the manufacture instructions. Total RNA was used for cDNA synthesis (PrimeScript RT Reagent Kit; Takara Bio, Takara Bio, Kusatsu, Japan). Transcript expression was quantified by real-time qPCR using iQ SYBR Green supermix (Bio-Rad Laboratories, Hercules, CA, USA), as previously described (Fichman and Mittler, 2021a; Fichman et al., 2021), with the following primers:

APX2 (AT3G09640) 5'-TCATCCTGGTAGACTGGACAAA-3' and 5'-CACATCTCTTAGATGATCCACACC-3';

MYB30 (AT3G28910) 5'- CCACTTGGCGAAAAAGGCTC-3' and 5'-ACCCGCTAGCTGAGGAAGTA-3';

ZAT10 (AT1G27730) 5'- ACTAGCCACGTTAGCAGTAGC-3' and 5'-GTTGAAGTTTGACCGGAAGTC-3';

ZAT12 (AT5G59820) 5'- TGGGAAGAGAGTGGCTTGTTT-3' and 5'-TAAACTGTTCTTCCAAGCTCCA-3';

ZHD5 (AT1G75240) 5' - CCACCAATCCAAGTCTCCCTC-3' and 5'-GCTCGCCGCATGATTCTTTAG-3' and

Elongation factor 1 alpha (5'-GAGCCCAAGTTTTTGAAGA-3' and 5'-TAAACTGTTCTTCCAAGCTCCA-3') was used for normalization of relative transcript levels. Results in the exponent of base 2 delta-delta terminal cycle were obtained by normalizing the relative transcript and comparing it to control WT from local leaf. Data represents 12 biological repeats and 3 technical repeats for each reaction. Standard error and Student t-test were calculated with Microsoft Excel.

ZAT12 promoter activity

Expression of luciferase driven by the *ZAT12* promoter was detected by luminescence imaging (Miller et al., 2009; Zandalinas et al., 2020b). Plants were sprayed with 1 mM luciferin (Gold Bio, St. Louis, MO, USA), and a single leaf was exposed to HL stress for 2 min (1700 µmol photons $s^{-1}m^{-2}$; ColdVision fiber optic LED light source; Schott, Southbridge, MA, USA). Plants were then imaged with the IVIS Lumina S5 apparatus (PerkinElmer, Waltham, MA, USA), as described before (Zandalinas et al., 2020b). Results are presented as precent of control (0 min). Each data set includes standard error of 8-12 technical repeats.

Statistical analysis

All experiments were repeated at least three times with at least three biological repeats. Graphs were generated with Microsoft Excel and are box plots with x as mean ± SE. P values (*$p < 0.05$, **$P < 0.01$, ***$P < 0.001$) were generated with two-tailed Student t-test paired samples. ANOVA followed by a Tukey's HSD post hoc test was used for hypothesis testing (different letters denote statistical significance at $p < 0.05$; Supplemental Table 2).

673 **Accession Numbers**

674

675 *HPCA1*- AT5G49760, *APX2* - AT3G09640, *CBL4* - AT5G24270, *CIPK26* - AT5G21326, *MYB30*
676 - AT3G28910, *OST1* - AT4G33950, *MSL3* -AT1G58200, *RBOHD* - AT5G47910, *RBOHF* -
677 AT1G64060, *ZAT10* - AT1G27730, *ZAT12* - AT5G59820, *ZHD5* - AT1G75240

678

679

680 **SUPPLEMENTAL DATA**

681

682 **Supplemental Table 1.** List of mutants that were screened for the presence or absence of the
683 systemic ROS wave in response to a local highlight stress applied to a single leaf.

684 **Supplemental Figure 1.** MSL3 is required for systemic cell-to-cell calcium signaling in response
685 to hydrogen peroxide. *Arabidopsis* plants were subjected to mock or 1 mM H_2O_2 treatment of a
686 single local leaf for 2 min and cytosolic calcium accumulation was imaged using Fluo-4-AM in
687 whole plants (local and systemic tissues). Representative time-lapse images of whole plant
688 cytosolic calcium accumulation in WT and *msl3-1* plants are shown alongside bar graphs of
689 combined data from all plants used for the analysis at the 0- and 30-min time points (local and
690 systemic). All experiments were repeated at least 3 times with 10 plants of each genotype per
691 experiment. Data is presented as box plot graphs; X is mean ± S.E., N=30, **P < 0.01, ***P <
692 0.001, Student t-test. Scale bar, 1 cm. In support of Figure 2. Abbreviations: MSL3,
693 mechanosensitive ion channel like 3; WT, wild-type.

694 **Supplemental Figure 2.** RBOHD is required for systemic cell-to-cell ROS signal initiation and
695 propagation, while RBOHF is required for systemic signal propagation. Representative time-lapse
696 images of ROS accumulation in stock and scion parts of grafted plants, generated using WT,
697 *rbohD*, or *rbohF* plants, in response to HL stress applied to a single leaf (indicated with a red
698 circle) belonging to the stock part. Scions are indicated by solid white lines, and stocks are
699 indicated by dashed white lines. ROS accumulation was imaged using H_2DCFDA. Scale bar, 1
700 cm. In support of Figure 5. Abbreviations: H_2DCFDA, 2',7'-dichlorodihydrofluorescein diacetate;

RBOHD, respiratory burst oxidase homolog D; RBOHF, respiratory burst oxidase homolog F; ROS, reactive oxygen species; WT, wild-type.

Supplemental Figure 3. HPCA1 or MSL3 are not required for systemic cell-to-cell calcium responses to salt stress. *Arabidopsis* plants were subjected to mock or 100 mM NaCl treatment of a single local leaf (red circle) and cytosolic calcium accumulation was imaged using Fluo-4-AM in whole plants (local and systemic tissues). Representative time-lapse images of whole plant cytosolic calcium accumulation in WT and *msl3-1* plants are shown alongside bar graphs of combined data from all plants used for the analysis at the 0- and 30-min time points (local and systemic). All experiments were repeated at least 3 times with 10 plants of each genotype per experiment. Data is presented as box plot graphs; X is mean ± S.E., N=30, *P < 0.05, **P < 0.01, Student t-test. Scale bar, 1 cm. In support of Figure 6. Abbreviations: HPCA1, H_2O_2-induced Ca^{2+} increases 1; MSL3, mechanosensitive ion channel like 3; WT, wild-type.

Supplemental Figure 4. Imaging of ROS, calcium, and membrane potential in wild-type plants subjected to a HL stress treatment applied to a single leaf. *Arabidopsis* plants were untreated or subjected to a high light (HL) stress treatment applied to a single leaf (Local; indicated with a red circle), and ROS (A), calcium (B), or membrane potential (C) were imaged, using H_2DCFDA, Fluo-4-AM, or DiBAC$_4$(3), respectively, in whole plants (local and systemic tissues) as described in Fichman and Mittler (2021a), and the Methods section. Scale bar, 1 cm. In support of Figures 1-3. Abbreviations: DiBAC$_4$(3), Bis-(1,3-Dibutylbarbituric Acid)Trimethine Oxonol; H_2DCFDA, 2',7'-dichlorodihydrofluorescein diacetate; HL, high light; ROS, reactive oxygen species; WT, wild-type.

Supplemental Movie 1. Live whole plant imaging of changes in cell-to-cell reactive oxygen species, calcium, and membrane potential signals in response to the application of high light stress to a single leaf (indicated by a white circle) of wild type and two independent mutants of HPCA1 (*hpca1-1*, *hpca1-2*). Note that although the detection of changes in cytosolic calcium levels precedes that of reactive oxygen species, cell-to-cell changes in calcium levels are dependent on reactive oxygen species sensing by HPCA1. By contrast, cell-to-cell changes in membrane potential do not require HPCA1. In support of Figures 1-3.

ACKNOWLEDGEMENTS

We thank The Arabidopsis Biological Resource Center (ABRC), and Professors E.E. Farmer, S. Karpinski, E. Liscum, C. Maurel, S. Pandey, A. S. Richter, G. Stacey and S. Zhang for seeds that were used for the screens shown in Supplemental Table 1.

FUNDING

National Science Foundation grants IOS-2110017, IOS-1932639; Interdisciplinary Plant Group, University of Missouri.

AUTHOR CONTRIBUTION

Conceptualization: RM, YF, SIZ; Investigation: YF, SIZ; Visualization: YF, SIZ; Funding acquisition: RM; Resources: SL, SP, RM; Writing – original draft: RM, YF; Writing – review & editing: RM, YF, SIZ, SL, SP.

COMPETING INTERESTS

The authors declare no competing interests

DATA AND MATERIALS AVAILABILITY

All data and materials are available upon request from RM (mittlerr@missouri.edu).

REFERENCES

Aguirre, J., and Lambeth, J. D. (2010). Nox enzymes from fungus to fly to fish and what they tell us about Nox function in mammals. Free Radic. Biol. Med. 49:1342–1353.

Alonso, J. M., Stepanova, A. N., Leisse, T. J., Kim, C. J., Chen, H., Shinn, P., Stevenson, D. K., Zimmerman, J., Barajas, P., Cheuk, R., et al. (2003). Genome-wide insertional mutagenesis of Arabidopsis thaliana. Science 301:653–657.

Clough, S. J., and Bent, A. F. (1998). Floral dip: a simplified method for Agrobacterium - mediated transformation of *Arabidopsis thaliana*. Plant J. 16:735–743.

Devireddy, A. R., Liscum, E., and Mittler, R. (2020) Phytochrome B Is Required for Systemic Stomatal Responses and Reactive Oxygen Species Signaling during Light Stress. Plant Physiol. 184:1563-1572.

Dickinson, M. S., Lu, J., Gupta, M., Marten, I., Hedrich, R., and Stroud, R. M. (2022). Molecular basis of multistep voltage activation in plant two-pore channel 1. Proc. Natl. Acad. Sci. U.S.A. 119:e2110936119.

Drerup, M. M., Schlücking, K., Hashimoto, K., Manishankar, P., Steinhorst, L., Kuchitsu, K., and Kudla, J. (2013). The calcineurin B-like calcium sensors CBL1 and CBL9 together with their interacting protein kinase CIPK26 regulate the Arabidopsis NADPH oxidase RBOHF. Mol. Plant 6:559–569.

Evans, M. J., Choi, W.-G., Gilroy, S., and Morris, R. J. (2016). A ROS-assisted calcium wave dependent on the AtRBOHD NADPH oxidase and TPC1 cation channel propagates the systemic response to salt stress. Plant Physiol. 171:1771–1784.

Farmer, E. E., Gao, Y.-Q., Lenzoni, G., Wolfender, J.-L., and Wu, Q. (2020). Wound- and mechanostimulated electrical signals control hormone responses. New Phytol. 227:1037–1050.

Fichman, Y., and Mittler, R. (2020a). Rapid systemic signaling during abiotic and biotic stresses: is the ROS wave master of all trades? Plant J. 102:887–896.

Fichman, Y., and Mittler, R. (2020b). Noninvasive live ROS imaging of whole plants grown in soil. Trends Plant Sci. 25:1052–1053.

Fichman, Y., Zandalinas, S. I., Sengupta, S., Burks, D., Myers, R. J. Jr, Azad, R. K., and Mittler, R. (2020c) MYB30 Orchestrates Systemic Reactive Oxygen Signaling and Plant Acclimation. Plant Physiol. 184:666-675.

Fichman, Y., and Mittler, R. (2021a). Integration of electric, calcium, reactive oxygen species and hydraulic signals during rapid systemic signaling in plants. Plant J. 107:7–20.

Fichman, Y., and Mittler, R. (2021b). A systemic whole-plant change in redox levels accompanies the rapid systemic response to wounding. Plant Physiol. 186:4–8.

787 Fichman, Y., Miller, G., and Mittler, R. (2019). Whole-plant live imaging of reactive oxygen
788 species. Mol. Plant 12:1203–1210.

789 Fichman, Y., Myers, R. J., Grant, D. G., and Mittler, R. (2021). Plasmodesmata-localized
790 proteins and ROS orchestrate light-induced rapid systemic signaling in Arabidopsis. Sci.
791 Signal. 14:eabf0322.

792 Fichman, Y., Xiong, H., Sengupta, S., Azad, R. K., Hibberd, J. M., Liscum, E., and Mittler, R.
793 (2022) Phytochrome B regulates reactive oxygen signaling during abiotic and biotic
794 stress in plants. bioRxiv 2021.11.29.470478; doi:
795 https://doi.org/10.1101/2021.11.29.470478

796 Gutteridge, J. M. C., and Halliwell, B. (2018). Mini-Review: Oxidative stress, redox stress or
797 redox success? Biochem. Biophys. Res. Commun. 502:183–186.

798 Hörandl, E., and Speijer, D. (2018). How oxygen gave rise to eukaryotic sex. Proc. Royal Soc. B
799 285:20172706.

800 Iwashita, H., Castillo, E., Messina, M. S., Swanson, R. A., and Chang, C. J. (2021). A tandem
801 activity-based sensing and labeling strategy enables imaging of transcellular hydrogen
802 peroxide signaling. Proc. Natl. Acad. Sci. U.S.A. 118:e2018513118.

803 Jabłońska, J., and Tawfik, D. S. (2021). The evolution of oxygen-utilizing enzymes suggests
804 early biosphere oxygenation. Nat Ecol Evol 5:442–448.

805 Johns, S., Hagihara, T., Toyota, M., and Gilroy, S. (2021). The fast and the furious: rapid long-
806 range signaling in plants. Plant Physiol. 185:694–706.

807 Karpinski, S., Reynolds, H., Karpinska, B., Wingsle, G., Creissen, G., and Mullineaux, P. (1999)
808 Systemic signaling and acclimation in response to excess excitation energy in
809 Arabidopsis. Science. 284:654-657.

810 Koncz, C., and Schell, J. (1986). The promoter of TL-DNA gene 5 controls the tissue-specific
811 expression of chimaeric genes carried by a novel type of Agrobacterium binary vector.
812 Molec Gen Genet 204:383–396.

813 Kromdijk, J., Głowacka, K., Leonelli, L., Gabilly, S. T., Iwai, M., Niyogi, K. K., and Long, S. P.
814 (2016) Improving photosynthesis and crop productivity by accelerating recovery from
815 photoprotection. Science. 354:857-861.

816 Laohavisit, A., Wakatake, T., Ishihama, N., Mulvey, H., Takizawa, K., Suzuki, T., and Shirasu,
817 K. (2020). Quinone perception in plants via leucine-rich-repeat receptor-like kinases.
818 Nature 587:92–97.

819 Luan, S., and Wang, C. (2021). Calcium Signaling Mechanisms Across Kingdoms. Annu. Rev.
820 Cell Dev. Biol. 37:311–340.

Lyzenga, W. J., Liu, H., Schofield, A., Muise-Hennessey, A., and Stone, S. L. (2013). Arabidopsis CIPK26 interacts with KEG, components of the ABA signalling network and is degraded by the ubiquitin–proteasome system. J. Exp.l Bot. 64:2779–2791.

Maurel, C., Tournaire-Roux, C., Verdoucq, L., and Santoni, V. (2021). Hormonal and environmental signaling pathways target membrane water transport. Plant Physiol. 187:2056–2070.

Miller, G., Schlauch, K., Tam, R., Cortes, D., Torres, M. A., Shulaev, V., Dangl, J. L., and Mittler, R. (2009). The plant NADPH oxidase RBOHD mediates rapid systemic signaling in response to diverse stimuli. Sci. Signal. 2:ra45–ra45.

Mittler, R. (2017). ROS are good. Trends Plant Sci. 22:11–19.

Mittler, R., Vanderauwera, S., Suzuki, N., Miller, G., Tognetti, V. B., Vandepoele, K., Gollery, M., Shulaev, V., and Van Breusegem, F. (2011). ROS signaling: the new wave? Trends Plant Sci. 16:300–309.

Mittler, R., Zandalinas, S. I., Fichman, Y., and Van Breusegem, F. (2022). ROS signalling in plant stress responses. Nat. Rev. Mol. Cell Biol. *In press*.

Mogami, J., Fujita, Y., Yoshida, T., Tsukiori, Y., Nakagami, H., Nomura, Y., Fujiwara, T., Nishida, S., Yanagisawa, S., Ishida, T., Takahashi, F., Morimoto, K., Kidokoro, S., Mizoi, J., Shinozaki, K., and Yamaguchi-Shinozaki, K. (2015) Two distinct families of protein kinases are required for plant growth under high external Mg^{2+} concentrations in Arabidopsis. Plant Physiol. 167:1039-1057.

Mousavi, S. A. R., Chauvin, A., Pascaud, F., Kellenberger, S., and Farmer, E. E. (2013). GLUTAMATE RECEPTOR-LIKE genes mediate leaf-to-leaf wound signalling. Nature 500:422–426.

Nguyen, C. T., Kurenda, A., Stolz, S., Chételat, A., and Farmer, E. E. (2018). Identification of cell populations necessary for leaf-to-leaf electrical signaling in a wounded plant. Proc. Natl. Acad. Sci. U.S.A. 115:10178–10183.

Nühse, T. S., Bottrill, A. R., Jones, A. M. E., and Peck, S. C. (2007). Quantitative phosphoproteomic analysis of plasma membrane proteins reveals regulatory mechanisms of plant innate immune responses. Plant J. 51:931–940.

Ogasawara, Y., Kaya, H., Hiraoka, G., Yumoto, F., Kimura, S., Kadota, Y., Hishinuma, H., Senzaki, E., Yamagoe, S., Nagata, K., et al. (2008). Synergistic activation of the Arabidopsis NADPH oxidase AtrbohD by Ca^{2+} and phosphorylation. J. Biol. Chem. 283:8885–8892.

Razzell, W., Evans, I. R., Martin, P., and Wood, W. (2013). Calcium flashes orchestrate the wound inflammatory response through DUOX activation and hydrogen peroxide release. Curr. Biol. 23:424–429.

Rodrigues, O., Reshetnyak, G., Grondin, A., Saijo, Y., Leonhardt, N., Maurel, C., and Verdoucq, L. (2017). Aquaporins facilitate hydrogen peroxide entry into guard cells to mediate ABA- and pathogen-triggered stomatal closure. Proc Natl Acad Sci USA 114:9200–9205.

Schieber, M., and Chandel, N. S. (2014). ROS Function in Redox Signaling and Oxidative Stress. Curr. Biol. 24:R453–R462.

Shao, Q., Gao, Q., Lhamo, D., Zhang, H., and Luan, S. (2020). Two glutamate- and pH-regulated Ca^{2+} channels are required for systemic wound signaling in Arabidopsis. Sci. Signal. 13:aba1453.

Sies, H., and Jones, D. P. (2020). Reactive oxygen species (ROS) as pleiotropic physiological signalling agents. Nat Rev Mol Cell Biol 21:363–383.

Sirichandra, C., Gu, D., Hu, H.-C., Davanture, M., Lee, S., Djaoui, M., Valot, B., Zivy, M., Leung, J., Merlot, S., et al. (2009). Phosphorylation of the Arabidopsis AtrbohF NADPH oxidase by OST1 protein kinase. FEBS Letters 583:2982–2986.

Slattery, R. A., Walker, B. J., Weber, A. P. M., and Ort, D. R. (2018) The Impacts of Fluctuating Light on Crop Performance. Plant Physiol. 176:990-1003.

Smirnoff, N., and Arnaud, D. (2019). Hydrogen peroxide metabolism and functions in plants. New Phytol. 221:1197–1214.

Suzuki, N., Miller, G., Salazar, C., Mondal, H. A., Shulaev, E., Cortes, D. F., Shuman, J. L., Luo, X., Shah, J., Schlauch, K., Shulaev, V., and Mittler, R. (2013) Temporal-spatial interaction between reactive oxygen species and abscisic acid regulates rapid systemic acclimation in plants. Plant Cell. 25:3553-3569.

Szechynska-Hebda, M., Lewandowska, M., Witoń, D., Fichman, Y., Mittler, R., and Karpinski, S. (2022). Aboveground plant-to-plant electrical signaling mediates network acquired acclimation. Plant Cell May 20:koac150. doi: 10.1093/plcell/koac150. Epub ahead of print. PMID: 35595231.

Taverne, Y. J., Merkus, D., Bogers, A. J., Halliwell, B., Duncker, D. J., and Lyons, T. W. (2018). Reactive oxygen species: Radical factors in the evolution of animal life. BioEssays 40:1700158.

Torres, M. A., Dangl, J. L., and Jones, J. D. G. (2002). Arabidopsis gp91phox homologues AtrbohD and AtrbohF are required for accumulation of reactive oxygen intermediates in the plant defense response. Proc. Natl. Acad. Sci. U.S.A. 99:517–522.

Toyota, M., Spencer, D., Sawai-Toyota, S., Jiaqi, W., Zhang, T., Koo, A. J., Howe, G. A., and Gilroy, S. (2018). Glutamate triggers long-distance, calcium-based plant defense signaling. Science 361:1112–1115.

Wang, P., Hsu, C.-C., Du, Y., Zhu, P., Zhao, C., Fu, X., Zhang, C., Paez, J. S., Macho, A. P., Tao, W. A., et al. (2020). Mapping proteome-wide targets of protein kinases in plant stress responses. Proc. Natl. Acad. Sci. U.S.A. 117:3270–3280.

Waszczak, C., Carmody, M., and Kangasjärvi, J. (2018). Reactive oxygen species in plant signaling. Annu Rev Plant Biol 69:209–236.

Wu, F., Chi, Y., Jiang, Z., Xu, Y., Xie, L., Huang, F., Wan, D., Ni, J., Yuan, F., Wu, X., et al. (2020). Hydrogen peroxide sensor HPCA1 is an LRR receptor kinase in Arabidopsis. Nature 578:577–581.

Yang, Y., Zhang, C., Tang, R.-J., Xu, H.-X., Lan, W.-Z., Zhao, F., and Luan, S. (2019). Calcineurin B-like proteins CBL4 and CBL10 mediate two independent salt tolerance pathways in Arabidopsis. Int. J. Mol. Sci. 20:2421.

Zandalinas, S. I., Fichman, Y., Devireddy, A. R., Sengupta, S., Azad, R. K., and Mittler, R. (2020a). Systemic signaling during abiotic stress combination in plants. Proc. Natl. Acad. Sci. U.S.A. 117:13810–13820.

Zandalinas, S. I., Fichman, Y., and Mittler, R. (2020b). Vascular bundles mediate systemic reactive oxygen signaling during light stress. Plant Cell 32:3425–3435.

Zheng, H., Kim, J., Liew, M., Yan, J. K., Herrera, O., Bok, J. W., Kelleher, N. L., Keller, N. P., and Wang, Y. (2015). Redox metabolites signal Polymicrobial biofilm development via the NapA oxidative stress cascade in Aspergillus. Curr. Biol. 25:29–37.

Zhu, J.-K. (2016). Abiotic stress signaling and responses in plants. Cell 167:313–324.

FIGURE LEGENDS

Figure 1. HPCA1 is required for systemic cell-to-cell ROS signaling in response to light stress. **(A)** *Arabidopsis* plants were subjected to a high light (HL) stress treatment applied to a single leaf (Local; indicated with a red circle), and ROS accumulation was imaged, using H_2DCFDA, in whole plants (local and systemic tissues). Representative time-lapse images of whole plant ROS accumulation in WT, *hpca1-1* and *hpca1-2* plants are shown alongside bar graphs of combined data from all plants used for the analysis at the 0- and 30-min time points (local and systemic). **(B)** Same as in (A), but for whole plant H_2O_2 accumulation that was imaged using Peroxy Orange 1 (PO1). **(C)** *Arabidopsis* plants were subjected to a HL stress treatment applied to a single leaf (Local) and the levels of H_2O_2 were measured in extracts from local and systemic leaves using Amplex®-Red. All experiments were repeated at least 3 times with 10 plants of each genotype per experiment. Data is presented as box plot graphs; X is mean ± S.E., N=30, *P < 0.05, **P < 0.01, ***P < 0.001, Student t-test. Scale bar, 1 cm. See movie S1 for live imaging. Abbreviations: H_2DCFDA, 2',7'-dichlorodihydrofluorescein diacetate; HPCA1, H_2O_2-induced Ca^{2+} increases 1; PO1, Peroxy Orange 1; ROS, reactive oxygen species; WT, wild-type.

Figure 2. HPCA1 and MSL3 are required for systemic cell-to-cell calcium signaling in response to light stress. **(A)** *Arabidopsis* plants were subjected to a high light (HL) stress treatment applied to a single leaf (Local; indicated with a red circle), and cytosolic calcium accumulation was imaged using Fluo-4-AM in whole plants (local and systemic tissues). Representative time-lapse images of whole plant cytosolic calcium accumulation in WT, *hpca1-1* and *hpca1-2* plants are shown alongside bar graphs of combined data from all plants used for the analysis at the 0- and 30-min time points (local and systemic). **(B)** Same as in (A), but for WT, *msl3-1* and *msl3-2* plants. Compared to WT, the *msl3-1* mutant is also deficient in cell-to-cell calcium signaling in response to a local application of H_2O_2 (Supplementary Figure 1). All experiments were repeated at least 3 times with 10 plants of each genotype per experiment. Data is presented as box plot graphs; X is mean ± S.E., N=30, *P < 0.05, **P < 0.01, Student t-test. Scale bar, 1 cm. See movie S1 for live imaging. Abbreviations: HPCA1, H_2O_2-induced Ca^{2+} increases 1; MSL3, mechanosensitive ion channel like 3; WT, wild-type.

Figure 3. HPCA1 is not required for systemic cell-to-cell changes in membrane potential in response to light stress. *Arabidopsis* plants were subjected to a high light (HL) stress treatment applied to a single leaf (Local; indicated with a red circle), and changes in membrane potential were imaged using $DiBAC_4(3)$ in whole plants (local and systemic tissues). Representative time-lapse images of whole plant changes in membrane potential in WT, *hpca1-1* and *hpca1-2* plants are shown alongside bar graphs of combined data from all plants used for the analysis at the 0- and 30-min time points (local and systemic). The double mutant *glr3.3 glr3.6*, that lacks a cell-to-cell membrane potential signal in response to HL stress (Fichman and Mittler 2021a), was used as a negative control. All experiments were repeated at least 3 times with 10 plants of each genotype per experiment. Data is presented as box plot graphs; X is mean ± S.E., N=30, **P < 0.01, Student t-test. Scale bar, 1 cm. See movie S1 for live imaging. Abbreviations: $DiBAC_4(3)$, Bis-(1,3-Dibutylbarbituric Acid) Trimethine Oxonol; GLR, glutamate receptor-like; HPCA1, H_2O_2-induced Ca^{2+} increases 1; WT, wild-type.

Figure 4. HPCA1 is required for local and systemic expression of stress-acclimation transcripts, as well as acclimation of plants to light stress. **(A)** Real-time quantitative PCR analysis of *APX2*, *MYB30*, *ZAT10*, *ZAT12*, and *ZHD5* expression in local and systemic leaves of wild-type and *hpca1-1* plants subjected to a local HL treatment. Transcripts tested were previously found to respond to HL stress in wild-type plants. Results are presented as relative quantity (RQ) compared to control WT from local leaf. **(B)** Averaged measurements of leaf injury (increase in ion leakage) of WT and *hpca1-1* plants. Measurements are shown for unstressed plants (control), local leaves subjected to a pretreatment of HL stress before a long HL stress period (local acclimation), systemic leaves of plants subjected to a local HL stress pretreatment before a long period of local HL stress was applied to a systemic leaf (systemic acclimation), and systemic leaves of plants subjected to a long HL stress period without pretreatment (HL without pretreatment). Results are presented as percent of control (leaves not exposed to HL stress). All experiments were repeated at least 3 times with 10 plants of each genotype per experiment. Data is presented in (A) as box plot graphs; X is mean ± S.E., N=30, *P < 0.05, **P < 0.01, ***P < 0.001, Student t-test. Data is presented in (B) as box plot graphs where X is mean ± S.E, N=30, one-way ANOVA followed by a Tukey test; lowercase letters donate significance (p < 0.05). Abbreviations: *APX2*, *ASCORBATE*

975 *PEROXIDASE 2*; HL, high light; HPCA1, H_2O_2-induced Ca^{2+} increases 1; *MYB30*,
976 *MYELOBLASTOSIS DOMAIN PROTEIN 30*; PCR, polymerase chain reaction; WT, wild-type;
977 *ZAT10*, *ZINC FINGER OF ARABIDOPSIS THALIANA 10*; *ZAT12; ZINC FINGER OF*
978 *ARABIDOPSIS THALIANA 12; ZHD5, ZINC FINGER HOMEODOMAIN 5*.

979

980 **Figure 5.** HPCA1 is required for systemic cell-to-cell ROS signal propagation, but not initiation,
981 in response to light stress. **(A)** Representative time-lapse images of ROS accumulation in stock
982 and scion parts of grafted plants, generated using WT and *hpca1-1* plants, in response to HL stress
983 applied to a single leaf (indicated with a red circle) belonging to the stock part. Scions are indicated
984 by solid white lines, and stocks are indicated by dashed white lines. **(B)** Bar graphs showing the
985 combined data from the stock and scion of grafted WT plants subjected to HL stress on a single
986 leaf of the stock scion. **(C)** Same as (B), but for different grafting combinations between WT and
987 *hpca1-1* plants. **(D)** Same as (B), but for different grafting combinations between WT and *rbohF*
988 plants. **(E)** Same as (B), but for different grafting combinations between WT and *rbohD* plants.
989 Representative time-lapse images of ROS accumulation in stock and scion parts of grafted WT
990 and *rbohD*, or *rbohF*, plants are shown in Supplementary Figure 2. All experiments were repeated
991 at least 3 times with 10 plants of each genotype per experiment. ROS accumulation was imaged
992 using H_2DCFDA. Data is presented as box plot graphs; X is mean ± S.E., N=30, *p < 0.05, **P <
993 0.01, ***P < 0.001, Student t-test. Scale bar, 1 cm. Abbreviations: H_2DCFDA, 2',7'-
994 dichlorodihydrofluorescein diacetate; HL, high light; HPCA1, H_2O_2-induced Ca^{2+} increases 1;
995 *rbohD,* respiratory burst oxidase homolog D; *rbohF,* respiratory burst oxidase homolog F; ROS,
996 reactive oxygen species; WT, wild-type.

997

998 **Figure 6.** HPCA1 is required for systemic cell-to-cell ROS responses to bacterial infection and
999 salt stress, but not wounding. **(A)** Representative time-lapse images of whole plant ROS
1000 accumulation in WT and *hpca1-1* plants subjected to mock or bacterial (*Pseudomonas syringae*
1001 DC3000) infection on a single local leaf are shown alongside bar graphs of combined data from
1002 all plants used for the analysis at the 0- and 30-min time points (local and systemic). **(B)** Same as
1003 in (A), but for mock and salt stress (100 mM NaCl) applied to a single local leaf. **(C)** Same as in

(A), but for wounding applied to a single local leaf (control plants were untreated). Although the *hpca1-1* mutant is deficient in cell-to-cell ROS signaling in response to salinity stress (B), it displays cell-to-cell calcium signaling in response to this stress (Supplementary Figure 3). All experiments were repeated at least 3 times with 10 plants of each genotype per experiment. ROS accumulation was imaged using H_2DCFDA. Data is presented as box plot graphs; X is mean ± S.E., N=30, **P < 0.01, Student t-test. Scale bar, 1 cm. Abbreviations: H_2DCFDA, 2',7'-dichlorodihydrofluorescein diacetate; HPCA1, H_2O_2-induced Ca^{2+} increases 1; ROS, reactive oxygen species; WT, wild-type.

Figure 7. CBL4, CIPK26, and OST1 are required for systemic cell-to-cell ROS signaling and acclimation to light stress. **(A)** Representative time-lapse images of whole plant ROS accumulation in wild-type (WT) and *cbl4-1* plants subjected to a local HL stress treatment (applied to a single local leaf; indicated with a red circle) are shown alongside bar graphs of combined data from all plants used for the analysis at the 0- and 30-min time points (local and systemic). **(B)** Same as (A), but for WT and *cipk26-2* plants. **(C)** Same as (A), but for WT and *ost1-2* plants. **(D)** Averaged measurements of leaf injury (increase in ion leakage) in WT, *cbl4*, *cipk26*, and *ost1* plants. Measurements are shown for unstressed plants (control), local leaves subjected to a pretreatment of HL stress before a long HL stress period (local acclimation), systemic leaves of plants subjected to a local HL stress pretreatment before a long period of local HL stress was applied to a systemic leaf (systemic acclimation), and systemic leaves of plants subjected to a long HL stress period without pretreatment (HL without pretreatment). All experiments were repeated at least 3 times with 10 plants of each genotype per experiment. ROS accumulation was imaged using H_2DCFDA. Data is presented in (A) to (C) as box plot graphs; X is mean ± S.E., N=30, **P < 0.01, Student t-test. Data is presented in (D) as box plot graphs; X is mean ± S.E., N=30, one-way ANOVA followed by a Tukey test; lowercase letters donate significance ($p < 0.05$). Scale bar, 1 cm. Abbreviations: CBL4, calcineurin B-like calcium sensor 4; CIPK26, CBL4-interacting protein kinase 26; H_2DCFDA, 2',7'-dichlorodihydrofluorescein diacetate; HL, high light; OST1, open stomata 1; ROS, reactive oxygen species; WT, wild-type.

Figure 8. CBL4, CIPK26, and OST1 are required for systemic ROS signal propagation, but not initiation, in response to light stress. **(A)** Representative time-lapse images of ROS accumulation in stock and scion parts of grafted plants, generated using WT and *cbl4-1* plants, in response to a local HL stress treatment applied to a single leaf (indicated with a red circle) belonging to the stock part. Scions are indicated by solid white lines, and stocks are indicated by dashed white lines. **(B)** Bar graphs showing the combined data from the stock and scion of grafted WT plants subjected to HL stress on a single leaf of the stock scion. **(C)** Same as (B), but for different grafting combinations between WT and *cbl4-1* plants. **(D)** Same as (B), but for different grafting combinations between WT and *cipk26-2* plants. **(E)** Same as (B), but for different grafting combinations between WT and *ost1-2* plants. All experiments were repeated at least 3 times with 10 plants of each genotype per experiment. ROS accumulation was imaged using H_2DCFDA. Data is presented as box plot graphs; X is mean ± S.E., N=30, **P < 0.01, ***P < 0.001, Student t-test. Scale bar, 1 cm. Abbreviations: CBL4, calcineurin B-like calcium sensor 4; CIPK26, CBL4-interacting protein kinase 26; H_2DCFDA, 2',7'-dichlorodihydrofluorescein diacetate; HL, high light; OST1, open stomata 1; ROS, reactive oxygen species; WT, wild-type.

Figure 9. Mutating specific amino acids in RBOHD suppresses systemic ROS accumulation in response to high light stress. **(A)** Representative time-lapse images of whole plant ROS accumulation in WT, *rbohD*, *rbohD* complemented with the wild type *RbohD* gene [*rbohD*/pRbohD::RbohD (genomic)], *rbohD* complemented with the *RbohD* cDNA expressed under the control of the *RbohD* promoter [*rbohD*/pRbohD::RbohD (cDNA)], *rbohD* complemented with the *RbohD* cDNA without the N-terminal regulatory domain (RD, 1-347) expressed under the control of the *RbohD* promoter [*rbohD*/pRboh::RbohD w/o RD], rbohD complemented with the *RbohD* gene with S22A and S26A mutations [*rbohD*/pRbohD::RbohD S22-26A], or *rbohD* complemented with the *RbohD* gene with S22A, S26A, S343A and S347A mutations [*rbohD*/pRbohD::RbohD S22-26-343-347A], following treatment of a single local leaf with HL stress (indicated with a red circle). **(B)** Bar graphs of combined data from all plants used for the analysis shown in (A) at the 0- and 30-min time points (systemic). **(C)** Bar graphs of combined *Zat12* promoter activity (luciferase imaging) in systemic leaves of *rbohD*/*Zat12::luciferase* double homozygous plants transformed with all vectors shown in (A),

measured at 0- and 30-min time following application of HL stress to a single local leaf. **(D)** Averaged measurements of leaf injury (increase in ion leakage) in systemic tissues of all lines shown in (A). Measurements are shown for unstressed systemic leaves (systemic control) and systemic leaves of plants subjected to a local HL stress pretreatment before a long period of local HL stress was applied to a systemic leaf (systemic acclimation). All experiments were repeated at least 3 times with 10 plants of each genotype per experiment. Two independent transgenic lines for each construct were averaged. ROS accumulation was imaged using H_2DCFDA. Data presented in (B) and (C) is mean ± S.E., N=30, *P < 0.05, Student t-test. Data presented in (D) is mean ± S.E., N=30, one-way ANOVA followed by a Tukey test; lowercase letters donate significance (p < 0.05). Scale bar, 1 cm. Abbreviations: cDNA, complementary DNA; H_2DCFDA, 2',7'-dichlorodihydrofluorescein diacetate; HL, high light; *RbohD,* respiratory burst oxidase homolog D; RD, regulatory domain; ROS, reactive oxygen species; WT, wild-type; *Zat12*, Zinc finger of *Arabidopsis thaliana* 12.

Figure 10. A model depicting the role of HPCA1 in the amplification and propagation of cell-to-cell ROS signaling in plants. HPCA1 is proposed to sense ROS at the apoplast and trigger an increase in cytosolic calcium levels via MSL3. The increase in calcium is proposed to activate a kinase cascade involving CBL4, CIPK26 and OST1 that activates RBOHD and RBOHF enhancing ROS production at the apoplast. The enhanced apoplastic ROS levels are sensed by the HPCA1 of the next cell in the cell-to-cell chain causing the enhanced apoplastic production of ROS by this cell, and a cell-to-cell ROS signaling process (the ROS wave) is formed. The enhanced apoplastic levels of ROS sensed by HPCA1 in each cell are also causing a positive amplification loop that further enhances ROS production in each cell of the cell-to-cell chain, including the initiating cell. ROS that accumulate in the apoplast (mainly H_2O_2) are shown to enter the cell via aquaporins and alter the redox state of different transcriptional regulators. The function of the pathway activated by HPCA1 is shown to be required for the enhanced transcript expression, acclimation, and resilience of plants to stress (please see text for more details). Dotted (for protein-protein interactions) and dashed (for regulatory effect) arrows are hypothetical. Abbreviations: APX2, Ascorbate peroxidase 2; HPCA1, H_2O_2-induced Ca^{2+} increases 1; CBL4, calcineurin B-like calcium sensor 4; CIPK26, CBL4-interacting protein kinase 26; MYB30, Myeloblastosis domain

protein 30; OST1, open stomata 1; PD, plasmodesmata; PDLP, plasmodesmata localized protein; phyB, phytochrome B; RBOHD, respiratory burst oxidase homolog D, RBOHF, respiratory burst oxidase homolog F; ROS, reactive oxygen species; ZAT12, Zinc finger of *Arabidopsis thaliana* 12.

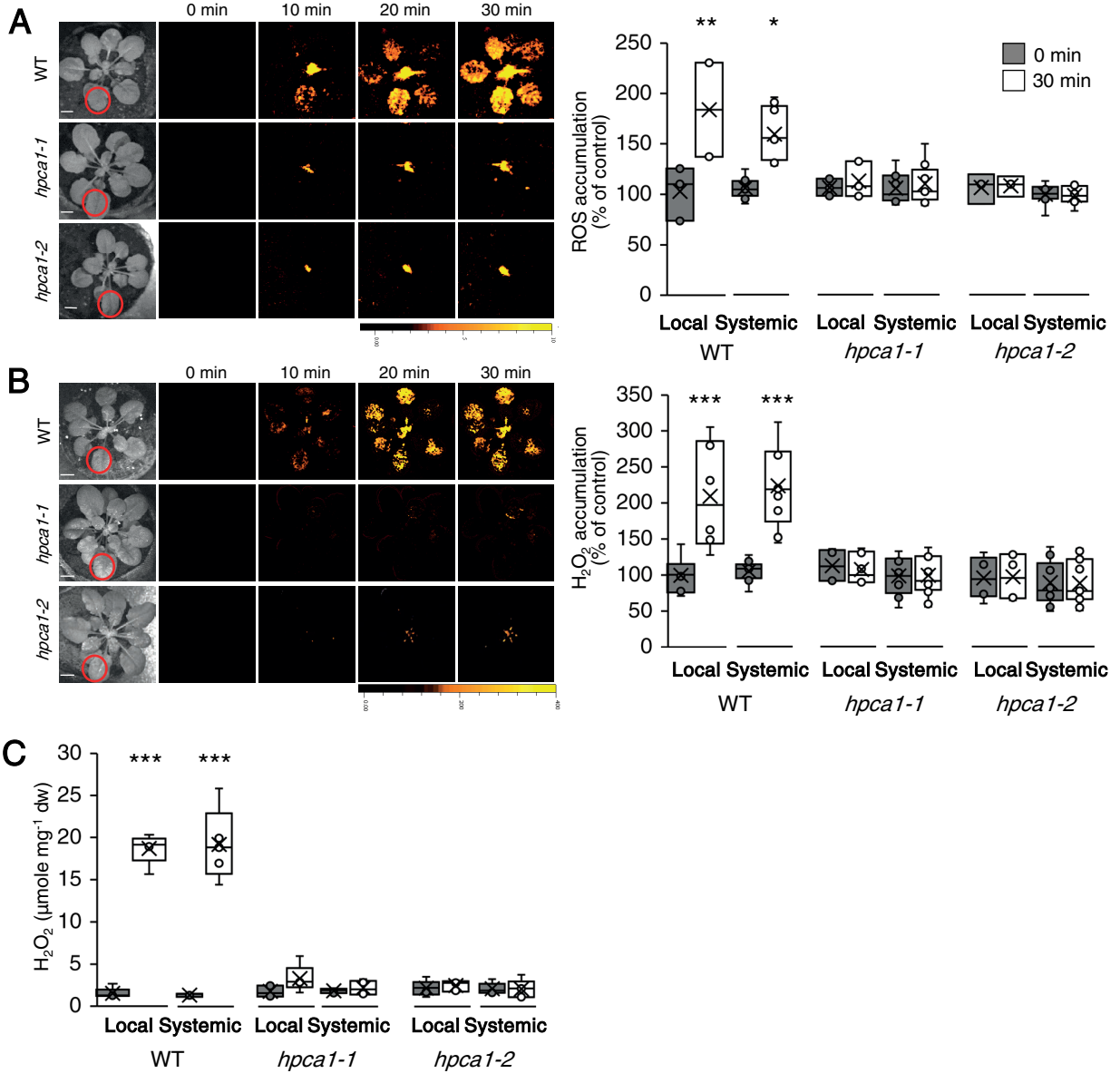

Figure 1. HPCA1 is required for systemic cell-to-cell ROS signaling in response to light stress. **(A)** *Arabidopsis* plants were subjected to a high light (HL) stress treatment applied to a single leaf (Local; indicated with a red circle), and ROS accumulation was imaged, using H_2DCFDA, in whole plants (local and systemic tissues). Representative time-lapse images of whole plant ROS accumulation in WT, *hpca1-1* and *hpca1-2* plants are shown alongside bar graphs of combined data from all plants used for the analysis at the 0- and 30-min time points (local and systemic). **(B)** Same as in (A), but for whole plant H_2O_2 accumulation that was imaged using Peroxy Orange 1 (PO1). **(C)** *Arabidopsis* plants were subjected to a HL stress treatment applied to a single leaf (Local) and the levels of H_2O_2 were measured in extracts from local and systemic leaves using Amplex®-Red. All experiments were repeated at least 3 times with 10 plants of each genotype per experiment. Data is presented as box plot graphs; X is mean ± S.E., N=30, *P < 0.05, **P < 0.01, ***P < 0.001, Student t-test. Scale bar, 1 cm. See movie S1 for live imaging. Abbreviations: H_2DCFDA, 2',7'-dichlorodihydrofluorescein diacetate; HPCA1, H_2O_2-induced Ca^{2+} increases 1; PO1, Peroxy Orange 1; ROS, reactive oxygen species; WT, wild-type.

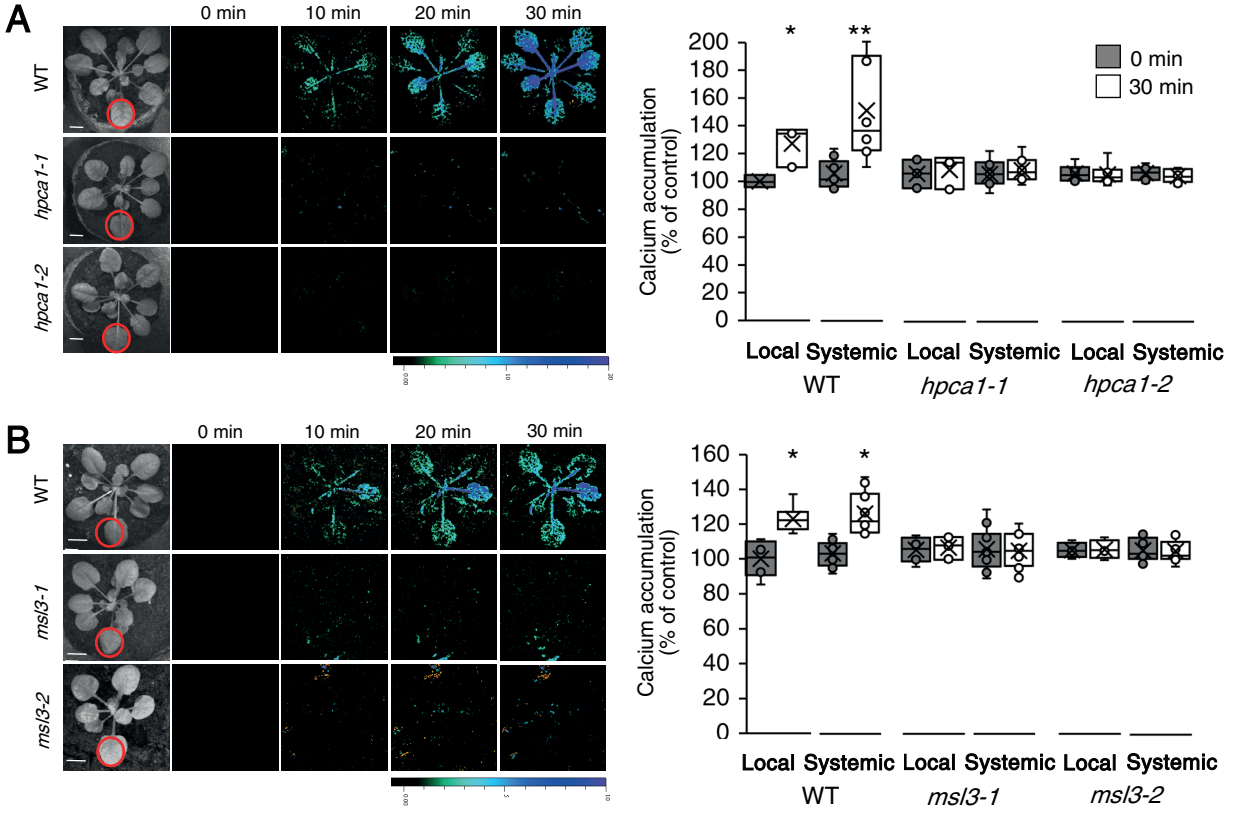

Figure 2. HPCA1 and MSL3 are required for systemic cell-to-cell calcium signaling in response to light stress. **(A)** *Arabidopsis* plants were subjected to a high light (HL) stress treatment applied to a single leaf (Local; indicated with a red circle), and cytosolic calcium accumulation was imaged using Fluo-4-AM in whole plants (local and systemic tissues). Representative time-lapse images of whole plant cytosolic calcium accumulation in WT, *hpca1-1* and *hpca1-2* plants are shown alongside bar graphs of combined data from all plants used for the analysis at the 0- and 30-min time points (local and systemic). **(B)** Same as in (A), but for WT, *msl3-1* and *msl3-2* plants. Compared to WT, the *msl3-1* mutant is also deficient in cell-to-cell calcium signaling in response to a local application of H_2O_2 (Supplementary Figure 1). All experiments were repeated at least 3 times with 10 plants of each genotype per experiment. Data is presented as box plot graphs; X is mean ± S.E., N=30, *P < 0.05, **P < 0.01, Student t-test. Scale bar, 1 cm. See movie S1 for live imaging. Abbreviations: HPCA1, H_2O_2-induced Ca^{2+} increases 1; MSL3, mechanosensitive ion channel like 3; WT, wild-type.

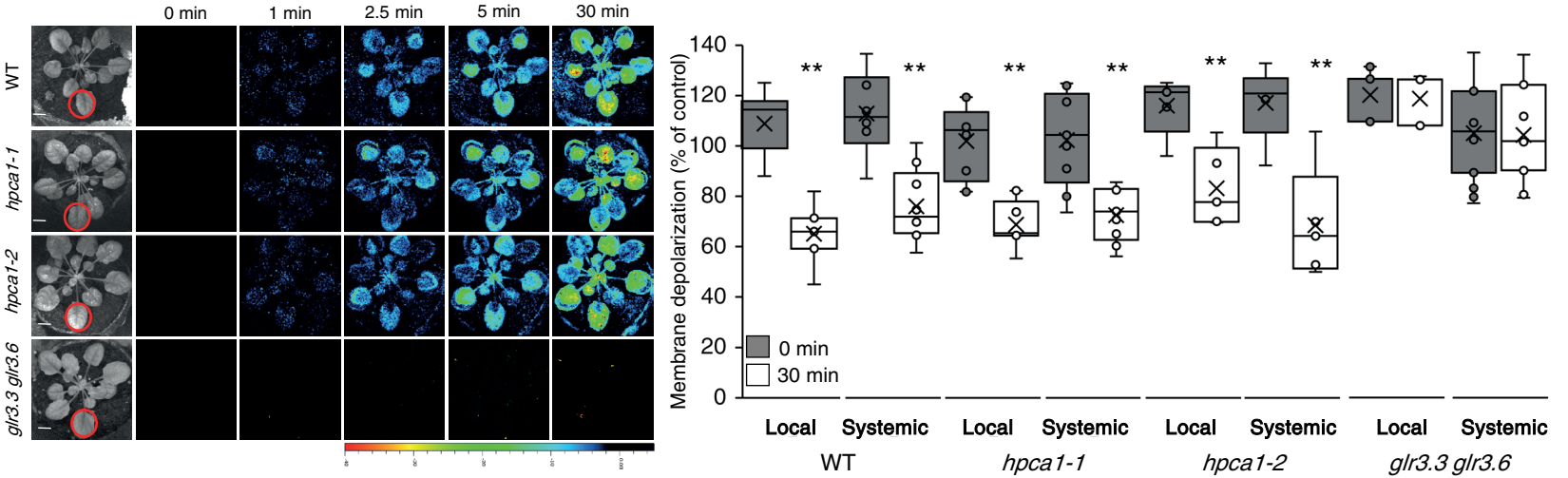

Figure 3. HPCA1 is not required for systemic cell-to-cell changes in membrane potential in response to light stress. *Arabidopsis* plants were subjected to a high light (HL) stress treatment applied to a single leaf (Local; indicated with a red circle), and changes in membrane potential were imaged using $DiBAC_4(3)$ in whole plants (local and systemic tissues). Representative time-lapse images of whole plant changes in membrane potential in WT, *hpca1-1* and *hpca1-2* plants are shown alongside bar graphs of combined data from all plants used for the analysis at the 0- and 30-min time points (local and systemic). The double mutant *glr3.3 glr3.6*, that lacks a cell-to-cell membrane potential signal in response to HL stress (Fichman and Mittler 2021a), was used as a negative control. All experiments were repeated at least 3 times with 10 plants of each genotype per experiment. Data is presented as box plot graphs; X is mean ± S.E., N=30, $^{**}P < 0.01$, Student t-test. Scale bar, 1 cm. See movie S1 for live imaging. Abbreviations: $DiBAC_4(3)$, Bis-(1,3-Dibutylbarbituric Acid) Trimethine Oxonol; GLR, glutamate receptor-like; HPCA1, H_2O_2-induced Ca^{2+} increases 1; WT, wild-type.

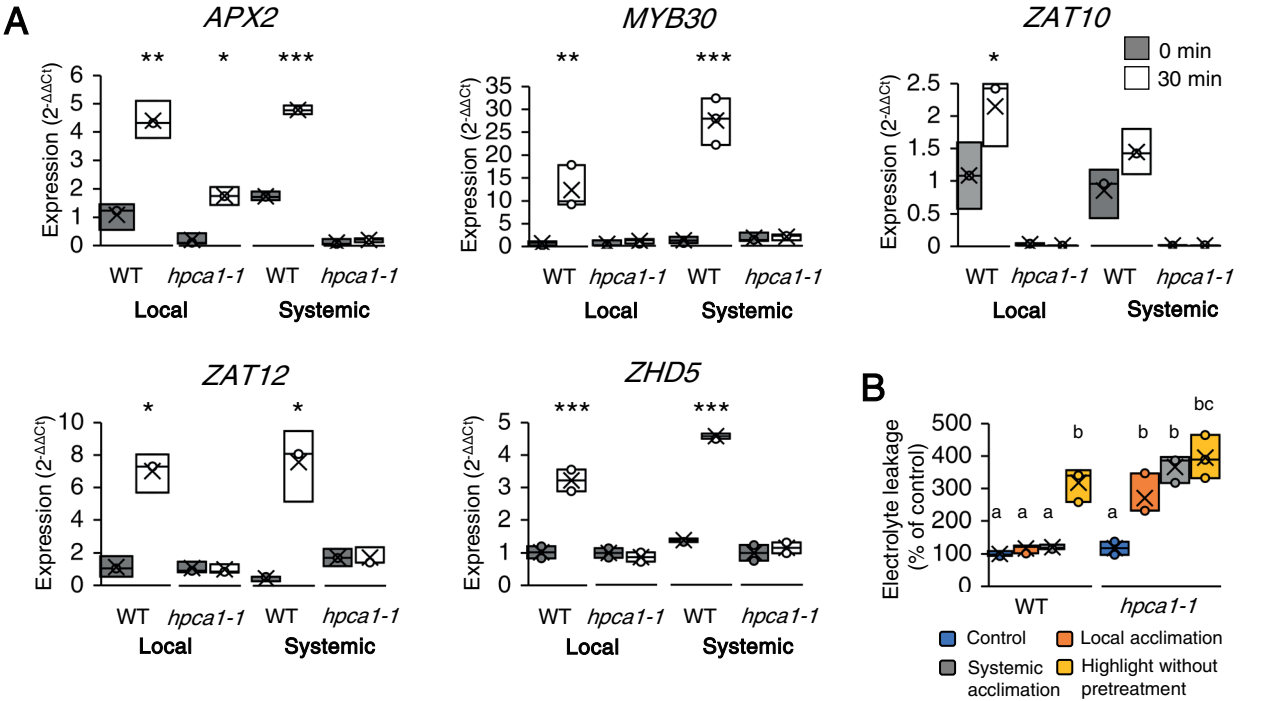

Figure 4. HPCA1 is required for local and systemic expression of stress-acclimation transcripts, as well as acclimation of plants to light stress. **(A)** Real-time quantitative PCR analysis of *APX2*, *MYB30*, *ZAT10*, *ZAT12*, and *ZHD5* expression in local and systemic leaves of wild-type and *hpca1-1* plants subjected to a local HL treatment. Transcripts tested were previously found to respond to HL stress in wild-type plants. Results are presented as relative quantity (RQ) compared to control WT from local leaf. **(B)** Averaged measurements of leaf injury (increase in ion leakage) of WT and *hpca1-1* plants. Measurements are shown for unstressed plants (control), local leaves subjected to a pretreatment of HL stress before a long HL stress period (local acclimation), systemic leaves of plants subjected to a local HL stress pretreatment before a long period of local HL stress was applied to a systemic leaf (systemic acclimation), and systemic leaves of plants subjected to a long HL stress period without pretreatment (HL without pretreatment). Results are presented as percent of control (leaves not exposed to HL stress). All experiments were repeated at least 3 times with 10 plants of each genotype per experiment. Data is presented in (A) as box plot graphs; X is mean ± S.E., N=30, *P < 0.05, **P < 0.01, ***P < 0.001, Student t-test. Data is presented in (B) as box plot graphs where X is mean ± S.E, N=30, one-way ANOVA followed by a Tukey test; lowercase letters donate significance (p < 0.05). Abbreviations: *APX2*, *ASCORBATE PEROXIDASE 2*; HL, high light; HPCA1, H_2O_2-induced Ca^{2+} increases 1; *MYB30*, *MYELOBLASTOSIS DOMAIN PROTEIN 30*; PCR, polymerase chain reaction; WT, wild-type; *ZAT10*, *ZINC FINGER OF ARABIDOPSIS THALIANA 10*; *ZAT12; ZINC FINGER OF ARABIDOPSIS THALIANA 12; ZHD5, ZINC FINGER HOMEODOMAIN 5*.

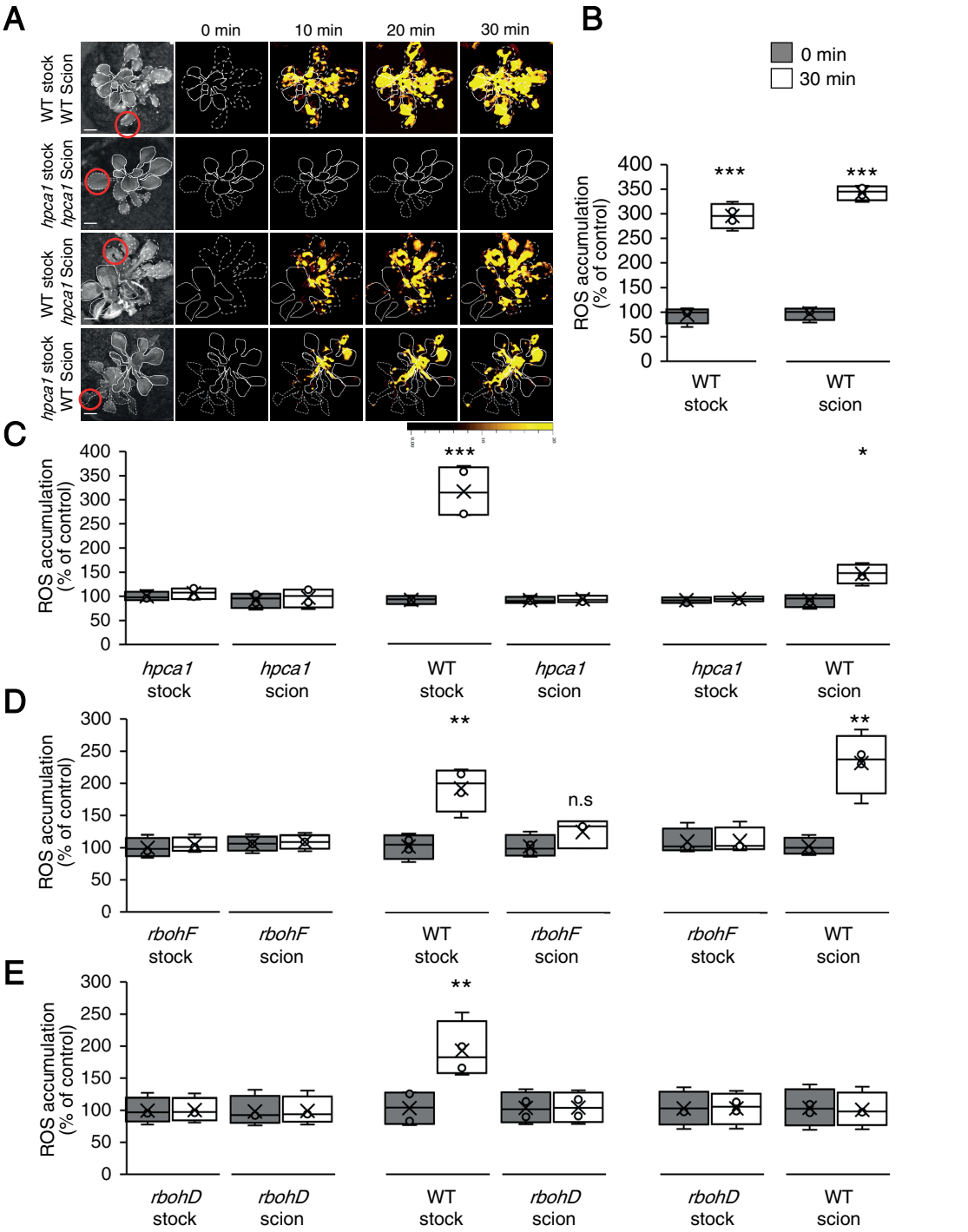

Figure 5. HPCA1 is required for systemic cell-to-cell ROS signal propagation, but not initiation, in response to light stress. **(A)** Representative time-lapse images of ROS accumulation in stock and scion parts of grafted plants, generated using WT and *hpca1-1* plants, in response to HL stress applied to a single leaf (indicated with a red circle) belonging to the stock part. Scions are indicated by solid white lines, and stocks are indicated by dashed white lines. **(B)** Bar graphs showing the combined data from the stock and scion of grafted WT plants subjected to HL stress on a single leaf of the stock scion. **(C)** Same as (B), but for different grafting combinations between WT and *hpca1-1* plants. **(D)** Same as (B), but for different grafting combinations between WT and *rbohF* plants. **(E)** Same as (B), but for different grafting combinations between WT and *rbohD* plants. Representative time-lapse images of ROS accumulation in stock and scion parts of grafted WT and *rbohD*, or *rbohF*, plants are shown in Supplementary Figure 2. All experiments were repeated at least 3 times with 10 plants of each genotype per experiment. ROS accumulation was imaged using H_2DCFDA. Data is presented as box plot graphs; X is mean ± S.E., N=30, *p < 0.05, **P < 0.01, ***P < 0.001, Student t-test. Scale bar, 1 cm. Abbreviations: H_2DCFDA, 2',7'-dichlorodihydrofluorescein diacetate; HL, high light; HPCA1, H_2O_2-induced Ca^{2+} increases 1; *rbohD,* respiratory burst oxidase homolog D; *rbohF,* respiratory burst oxidase homolog F; ROS, reactive oxygen species; WT, wild-type.

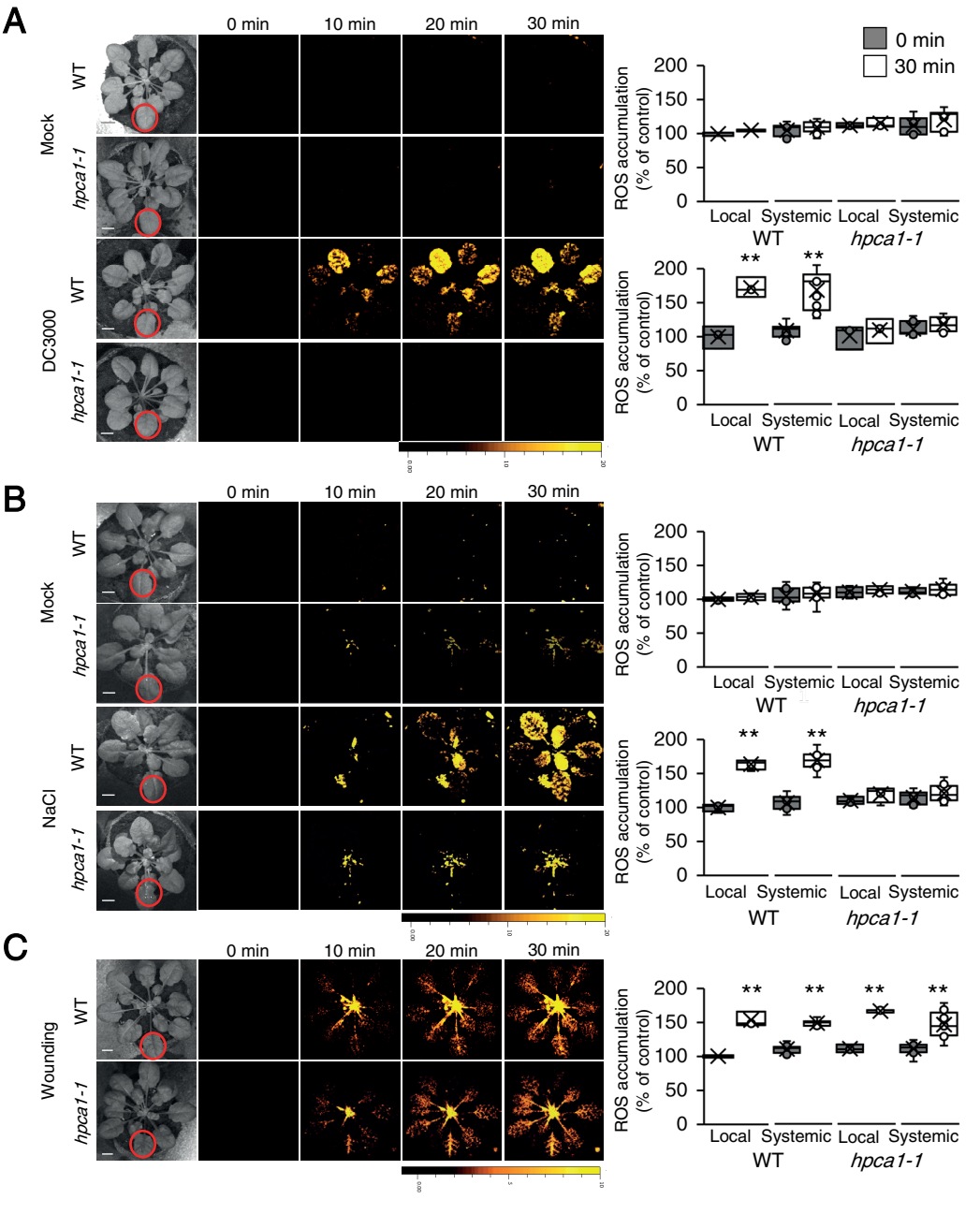

Figure 6. HPCA1 is required for systemic cell-to-cell ROS responses to bacterial infection and salt stress, but not wounding. **(A)** Representative time-lapse images of whole plant ROS accumulation in WT and *hpca1-1* plants subjected to mock or bacterial (*Pseudomonas syringae* DC3000) infection on a single local leaf are shown alongside bar graphs of combined data from all plants used for the analysis at the 0- and 30-min time points (local and systemic). **(B)** Same as in (A), but for mock and salt stress (100 mM NaCl) applied to a single local leaf. **(C)** Same as in (A), but for wounding applied to a single local leaf (control plants were untreated). Although the *hpca1-1* mutant is deficient in cell-to-cell ROS signaling in response to salinity stress (B), it displays cell-to-cell calcium signaling in response to this stress (Supplementary Figure 3). All experiments were repeated at least 3 times with 10 plants of each genotype per experiment. ROS accumulation was imaged using H_2DCFDA. Data is presented as box plot graphs; X is mean ± S.E., N=30, **P < 0.01, Student t-test. Scale bar, 1 cm. Abbreviations: HPCA1, H_2O_2-induced Ca^{2+} increases 1; ROS, reactive oxygen species; WT, wild-type.

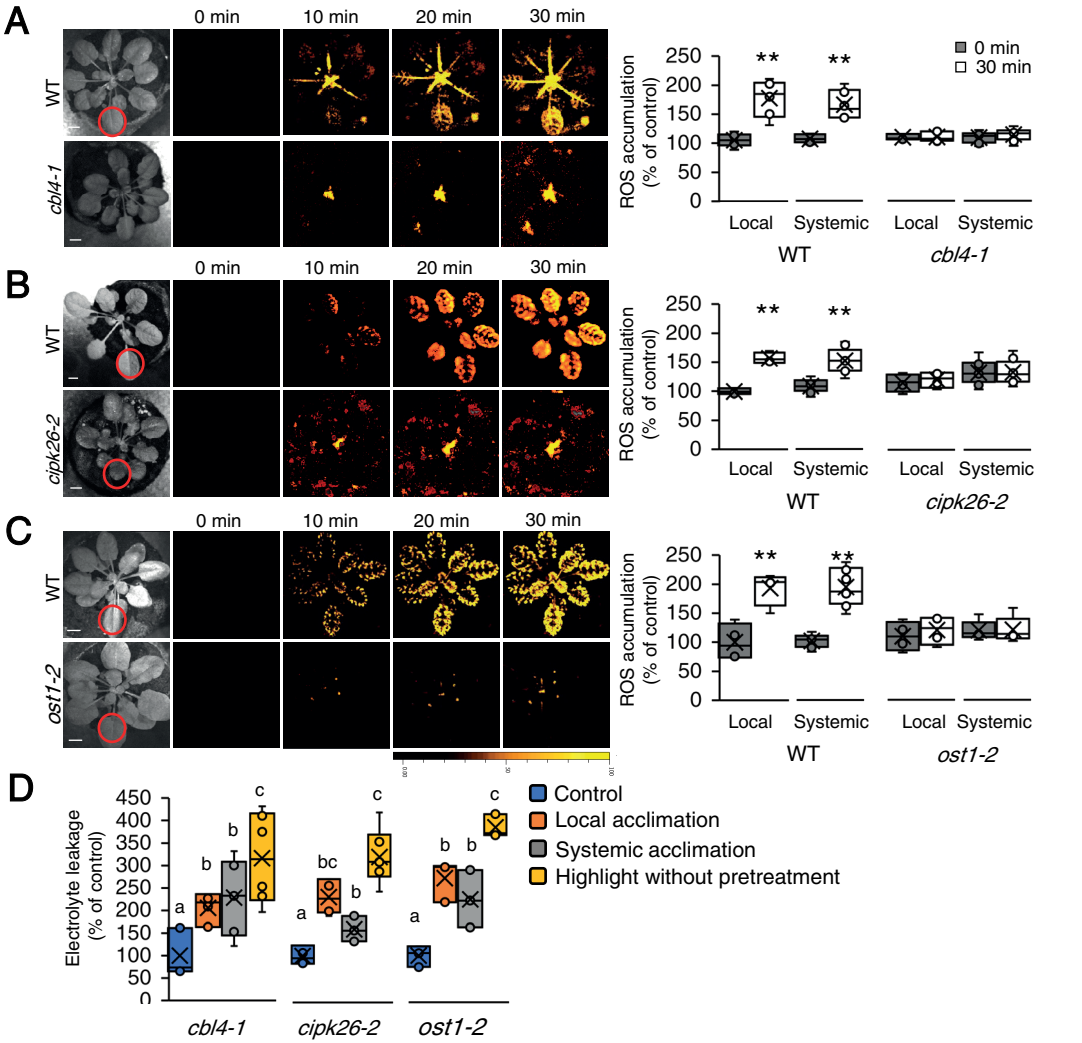

Figure 7. CBL4, CIPK26, and OST1 are required for systemic cell-to-cell ROS signaling and acclimation to light stress. **(A)** Representative time-lapse images of whole plant ROS accumulation in wild-type (WT) and *cbl4-1* plants subjected to a local HL stress treatment (applied to a single local leaf; indicated with a red circle) are shown alongside bar graphs of combined data from all plants used for the analysis at the 0- and 30-min time points (local and systemic). **(B)** Same as (A), but for WT and *cipk26-2* plants. **(C)** Same as (A), but for WT and *ost1-2* plants. **(D)** Averaged measurements of leaf injury (increase in ion leakage) in WT, *cbl4*, *cipk26*, and *ost1* plants. Measurements are shown for unstressed plants (control), local leaves subjected to a pretreatment of HL stress before a long HL stress period (local acclimation), systemic leaves of plants subjected to a local HL stress pretreatment before a long period of local HL stress was applied to a systemic leaf (systemic acclimation), and systemic leaves of plants subjected to a long HL stress period without pretreatment (HL without pretreatment). All experiments were repeated at least 3 times with 10 plants of each genotype per experiment. ROS accumulation was imaged using H_2DCFDA. Data is presented in (A) to (C) as box plot graphs; X is mean ± S.E., N=30, **P < 0.01, Student t-test. Data is presented in (D) as box plot graphs; X is mean ± S.E., N=30, one-way ANOVA followed by a Tukey test; lowercase letters donate significance ($p < 0.05$). Scale bar, 1 cm. Abbreviations: CBL4, calcineurin B-like calcium sensor 4; CIPK26, CBL4-interacting protein kinase 26; H_2DCFDA, 2',7'-dichlorodihydrofluorescein diacetate; HL, high light; OST1, open stomata 1; ROS, reactive oxygen species; WT, wild-type.

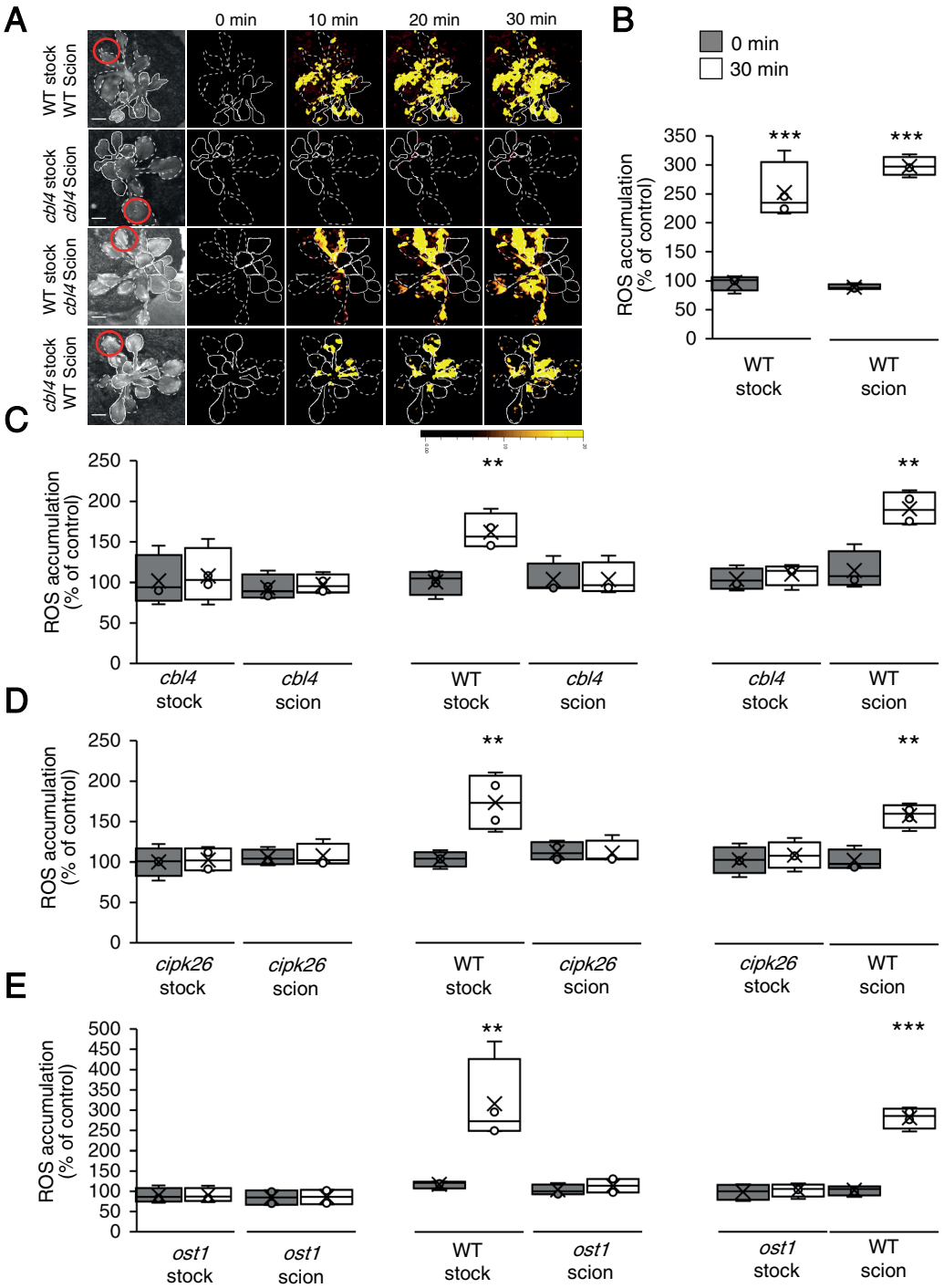

Figure 8. CBL4, CIPK26, and OST1 are required for systemic ROS signal propagation, but not initiation, in response to light stress. **(A)** Representative time-lapse images of ROS accumulation in stock and scion parts of grafted plants, generated using WT and *cbl4-1* plants, in response to a local HL stress treatment applied to a single leaf (indicated with a red circle) belonging to the stock part. Scions are indicated by solid white lines, and stocks are indicated by dashed white lines. **(B)** Bar graphs showing the combined data from the stock and scion of grafted WT plants subjected to HL stress on a single leaf of the stock scion. **(C)** Same as (B), but for different grafting combinations between WT and *cbl4-1* plants. **(D)** Same as (B), but for different grafting combinations between WT and *cipk26-2* plants. **(E)** Same as (B), but for different grafting combinations between WT and *ost1-2* plants. All experiments were repeated at least 3 times with 10 plants of each genotype per experiment. ROS accumulation was imaged using H_2DCFDA. Data is presented as box plot graphs; X is mean ± S.E., N=30, **P < 0.01, ***P < 0.001, Student t-test. Scale bar, 1 cm. Abbreviations: CBL4, calcineurin B-like calcium sensor 4; CIPK26, CBL4-interacting protein kinase 26; H_2DCFDA, 2',7'-dichlorodihydrofluorescein diacetate; HL, high light; OST1, open stomata 1; ROS, reactive oxygen species; WT, wild-type.

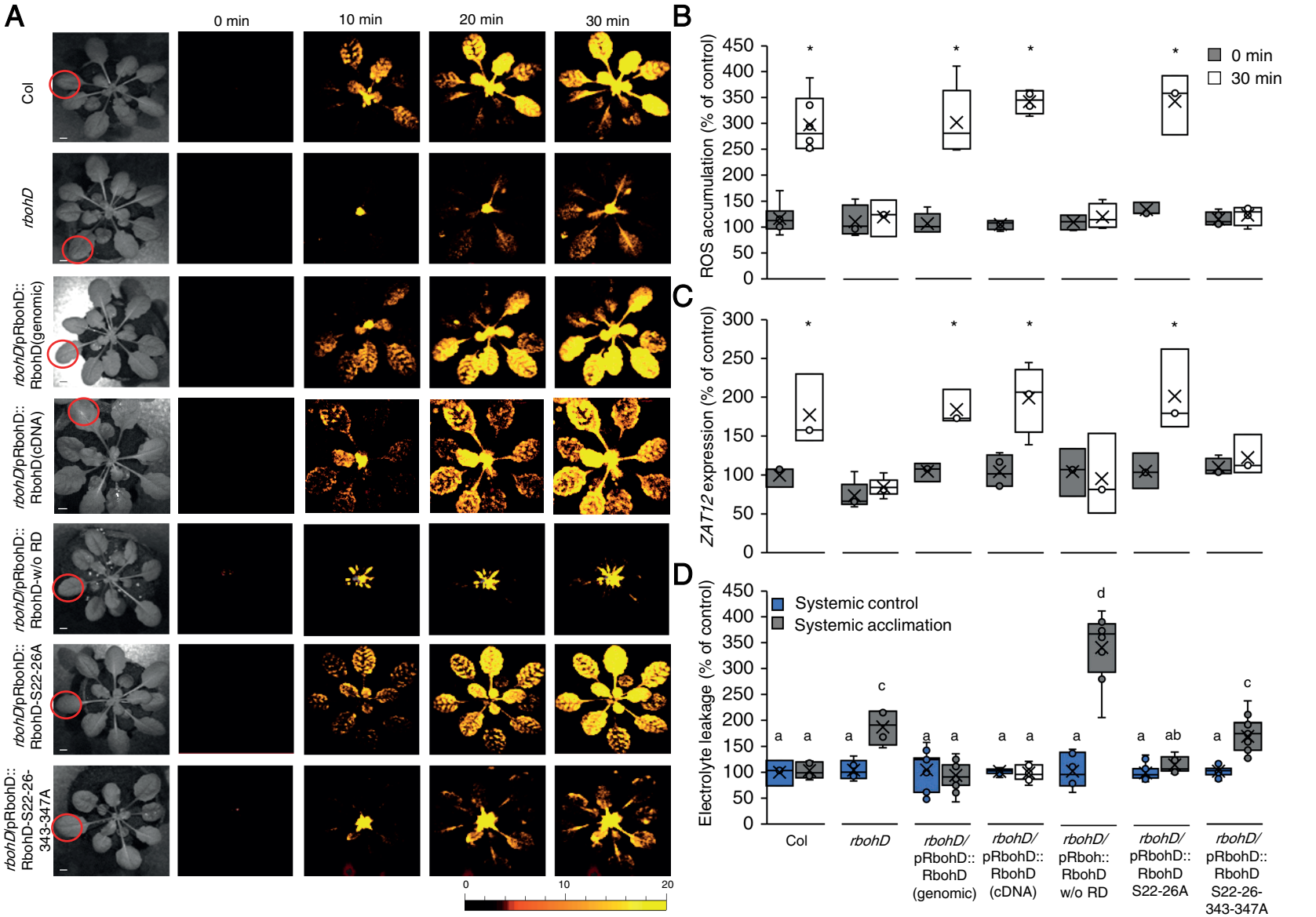

Figure 9. Mutating specific amino acids in RBOHD suppresses systemic ROS accumulation in response to high light stress. **(A)** Representative time-lapse images of whole plant ROS accumulation in WT, *rbohD*, *rbohD* complemented with the wild type *RbohD* gene [*rbohD*/pRbohD::RbohD (genomic)], *rbohD* complemented with the *RbohD* cDNA expressed under the control of the *RbohD* promoter [*rbohD*/pRbohD::RbohD (cDNA)], *rbohD* complemented with the *RbohD* cDNA without the N-terminal regulatory domain (RD, 1-347) expressed under the control of the *RbohD* promoter [*rbohD*/pRboh::RbohD w/o RD], rbohD complemented with the *RbohD* gene with S22A and S26A mutations [*rbohD*/pRbohD::RbohD S22-26A], or *rbohD* complemented with the *RbohD* gene with S22A, S26A, S343A and S347A mutations [*rbohD*/pRbohD::RbohD S22-26-343-347A], following treatment of a single local leaf with HL stress (indicated with a red circle). **(B)** Bar graphs of combined data from all plants used for the analysis shown in (A) at the 0- and 30-min time points (systemic). **(C)** Bar graphs of combined *Zat12* promoter activity (luciferase imaging) in systemic leaves of *rbohD*/*Zat12::luciferase* double homozygous plants transformed with all vectors shown in (A), measured at 0- and 30-min time following application of HL stress to a single local leaf. **(D)** Averaged measurements of leaf injury (increase in ion leakage) in systemic tissues of all lines shown in (A). Measurements are shown for unstressed systemic leaves (systemic control) and systemic leaves of plants subjected to a local HL stress pretreatment before a long period of local HL stress was applied to a systemic leaf (systemic acclimation). All experiments were repeated at least 3 times with 10 plants of each genotype per experiment. Two independent transgenic lines for each construct were averaged. ROS accumulation was imaged using H_2DCFDA. Data presented in (B) and (C) is mean ± S.E., N=30, *P < 0.05, Student t-test. Data presented in (D) is mean ± S.E., N=30, one-way ANOVA followed by a Tukey test; lowercase letters donate significance (p < 0.05). Scale bar, 1 cm. Abbreviations: cDNA, complementary DNA; H_2DCFDA, 2',7'-dichlorodihydrofluorescein diacetate; HL, high light; *RbohD,* respiratory burst oxidase homolog D; RD, regulatory domain; ROS, reactive oxygen species; WT, wild-type; *Zat12*, Zinc finger of *Arabidopsis thaliana* 12.

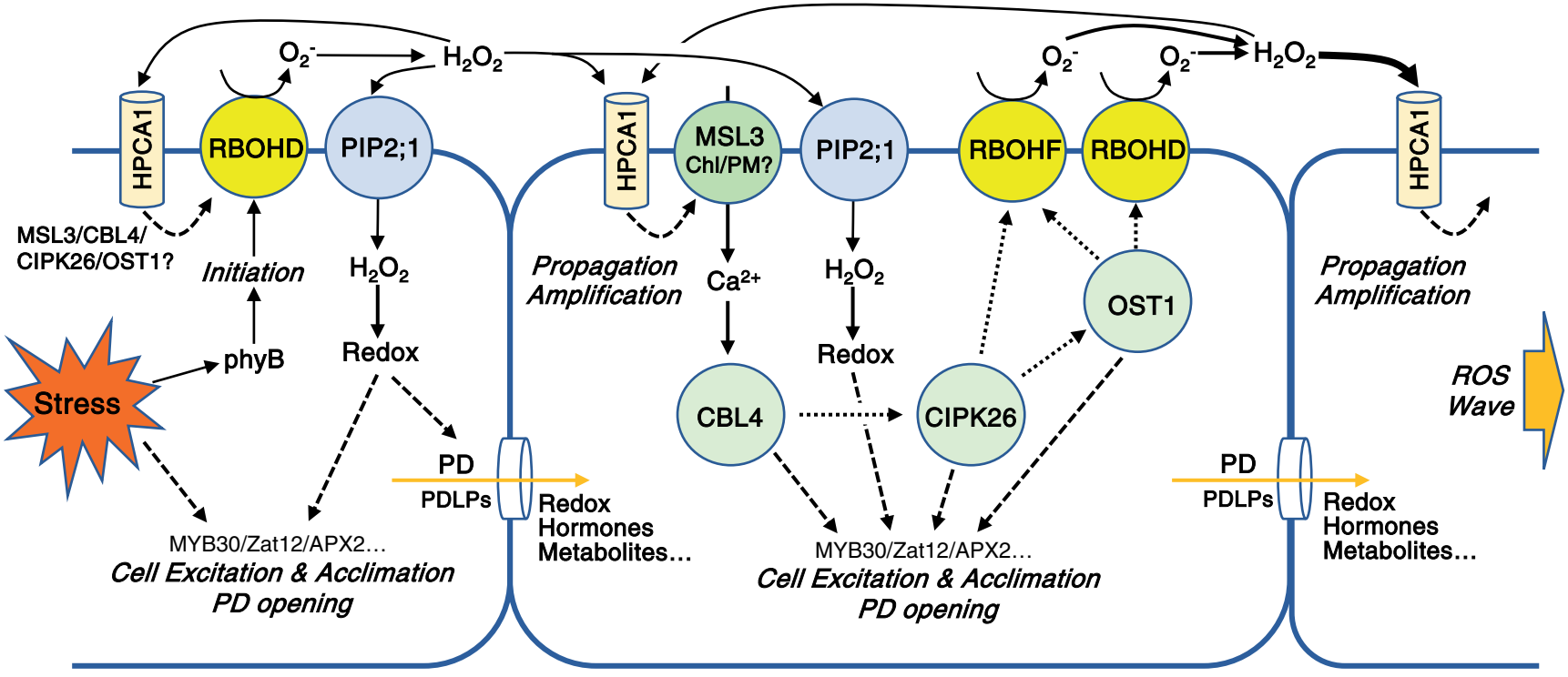

Figure 10. A model depicting the role of HPCA1 in the amplification and propagation of cell-to-cell ROS signaling in plants. HPCA1 is proposed to sense ROS at the apoplast and trigger an increase in cytosolic calcium levels via MSL3. The increase in calcium is proposed to activate a kinase cascade involving CBL4, CIPK26 and OST1 that activates RBOHD and RBOHF enhancing ROS production at the apoplast. The enhanced apoplastic ROS levels are sensed by the HPCA1 of the next cell in the cell-to-cell chain causing the enhanced apoplastic production of ROS by this cell, and a cell-to-cell ROS signaling process (the ROS wave) is formed. The enhanced apoplastic levels of ROS sensed by HPCA1 in each cell are also causing a positive amplification loop that further enhances ROS production in each cell of the cell-to-cell chain, including the initiating cell. ROS that accumulate in the apoplast (mainly H_2O_2) are shown to enter the cell via aquaporins and alter the redox state of different transcriptional regulators. The function of the pathway activated by HPCA1 is shown to be required for the enhanced transcript expression, acclimation, and resilience of plants to stress (please see text for more details). Dotted (for protein-protein interactions) and dashed (for regulatory effect) arrows are hypothetical. Abbreviations: APX2, Ascorbate peroxidase 2; HPCA1, H_2O_2-induced Ca^{2+} increases 1; CBL4, calcineurin B-like calcium sensor 4; CIPK26, CBL4-interacting protein kinase 26; MYB30, Myeloblastosis domain protein 30; OST1, open stomata 1; PD, plasmodesmata; PDLP, plasmodesmata localized protein; phyB, phytochrome B; RBOHD, respiratory burst oxidase homolog D, RBOHF, respiratory burst oxidase homolog F; ROS, reactive oxygen species; ZAT12, Zinc finger of *Arabidopsis thaliana* 12.

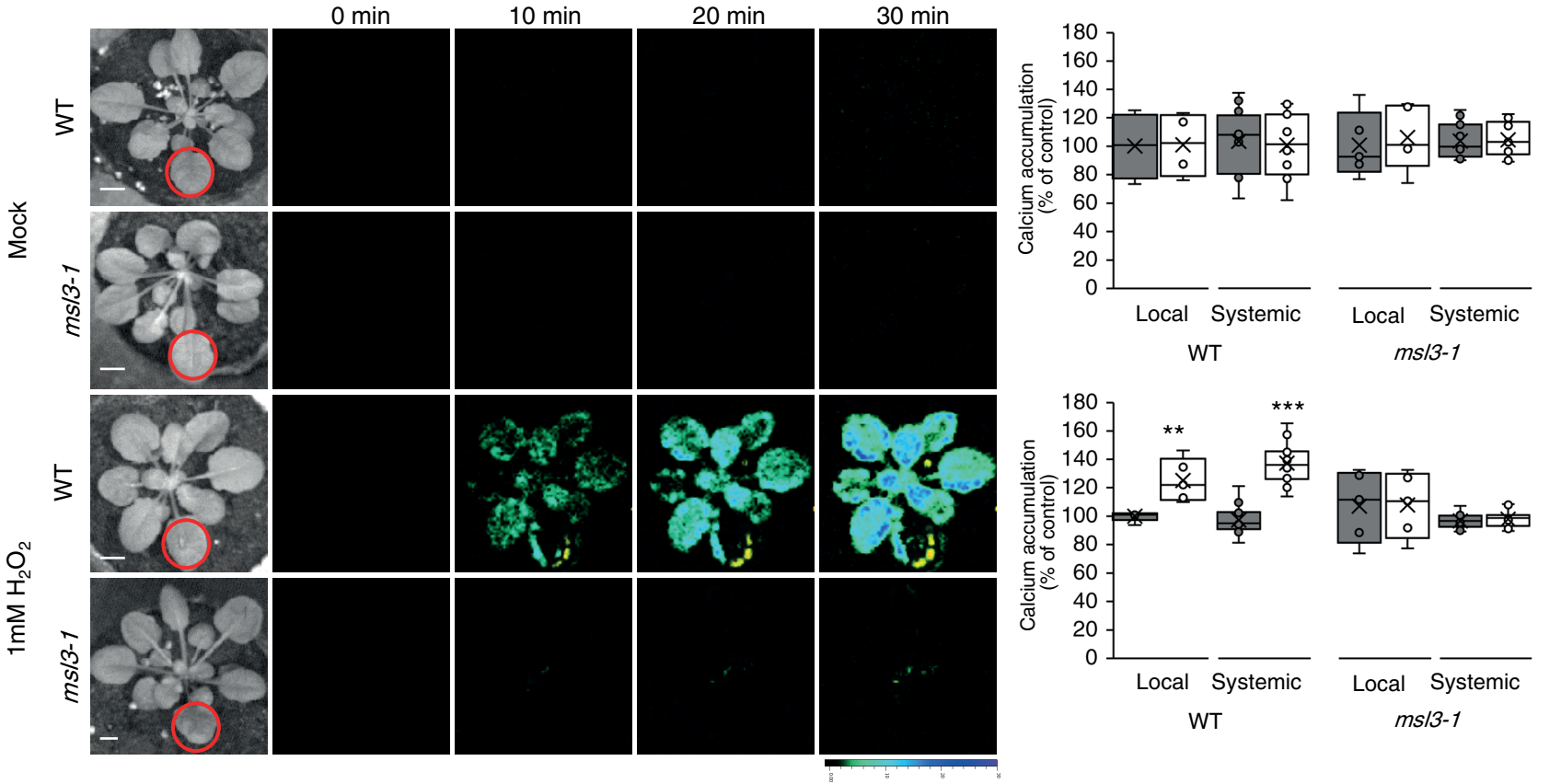

Supplemental Figure 1. MSL3 is required for systemic cell-to-cell calcium signaling in response to hydrogen peroxide. *Arabidopsis* plants were subjected to mock or 1 mM H_2O_2 treatment of a single local leaf for 2 min and cytosolic calcium accumulation was imaged using Fluo-4-AM in whole plants (local and systemic tissues). Representative time-lapse images of whole plant cytosolic calcium accumulation in WT and *msl3-1* plants are shown alongside bar graphs of combined data from all plants used for the analysis at the 0- and 30-min time points (local and systemic). All experiments were repeated at least 3 times with 10 plants of each genotype per experiment. Data is presented as box plot graphs; X is mean ± S.E., N=30, **P < 0.01, ***P < 0.001, Student t-test. Scale bar, 1 cm. In support of Figure 2. Abbreviations: MSL3, mechanosensitive ion channel like 3; WT, wild-type.

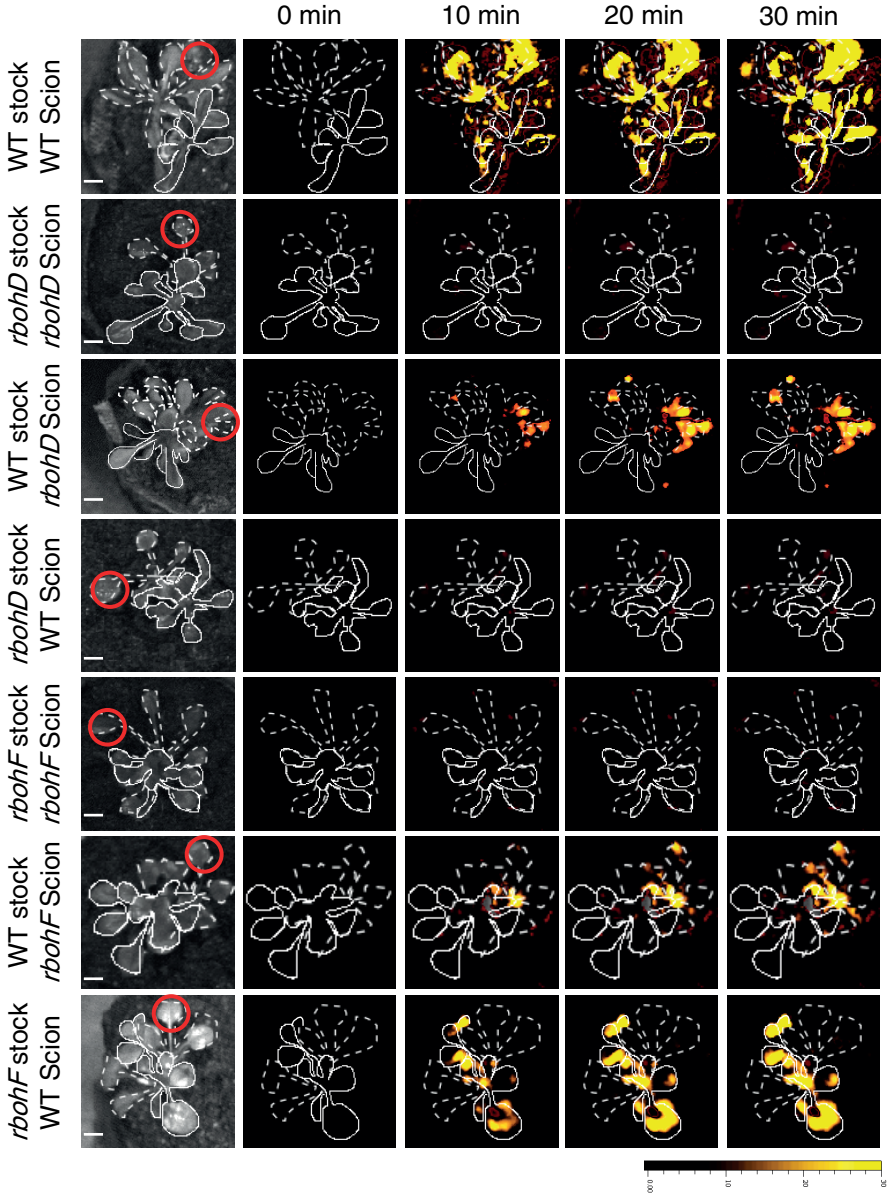

Supplemental Figure 2. RBOHD is required for systemic cell-to-cell ROS signal initiation and propagation, while RBOHF is required for systemic signal propagation. Representative time-lapse images of ROS accumulation in stock and scion parts of grafted plants, generated using WT, *rbohD*, or *rbohF* plants, in response to HL stress applied to a single leaf (indicated with a red circle) belonging to the stock part. Scions are indicated by solid white lines, and stocks are indicated by dashed white lines. ROS accumulation was imaged using H_2DCFDA. Scale bar, 1 cm. In support of Figure 5. Abbreviations: H_2DCFDA, 2',7'-dichlorodihydrofluorescein diacetate; RBOHD, respiratory burst oxidase homolog D; RBOHF, respiratory burst oxidase homolog F; ROS, reactive oxygen species; WT, wild-type.

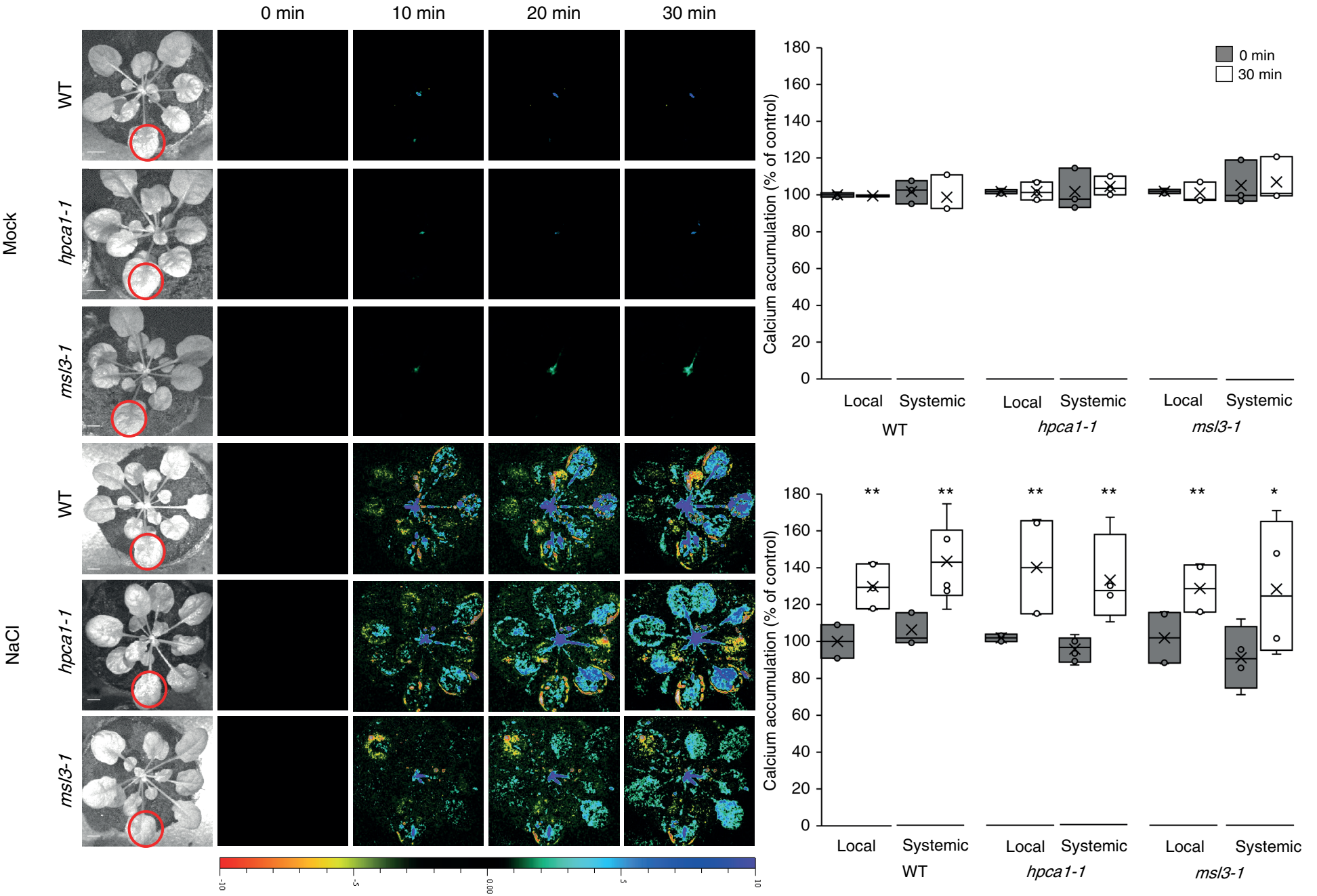

Supplemental Figure 3. HPCA1 or MSL3 are not required for systemic cell-to-cell calcium responses to salt stress. *Arabidopsis* plants were subjected to mock or 100 mM NaCl treatment of a single local leaf (red circle) and cytosolic calcium accumulation was imaged using Fluo-4-AM in whole plants (local and systemic tissues). Representative time-lapse images of whole plant cytosolic calcium accumulation in WT and *msl3-1* plants are shown alongside bar graphs of combined data from all plants used for the analysis at the 0- and 30-min time points (local and systemic). All experiments were repeated at least 3 times with 10 plants of each genotype per experiment. Data is presented as box plot graphs; X is mean ± S.E., N=30, *P < 0.05, **P < 0.01, Student t-test. Scale bar, 1 cm. In support of Figure 6. Abbreviations: HPCA1, H_2O_2-induced Ca^{2+} increases 1; MSL3, mechanosensitive ion channel like 3; WT, wild-type.

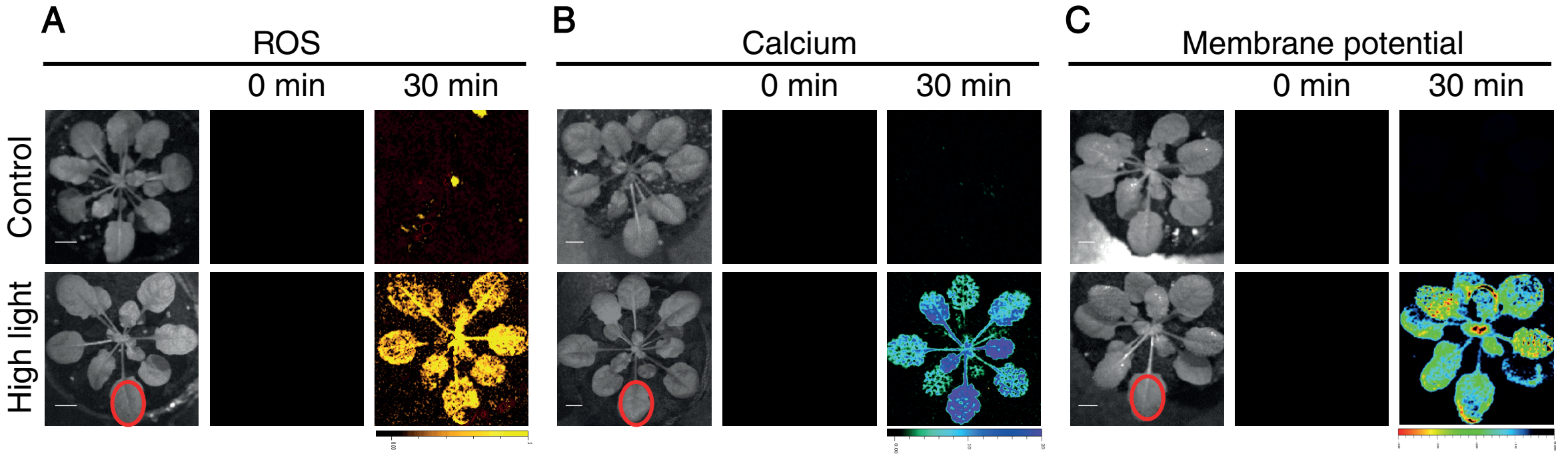

Supplemental Figure 4. Imaging of ROS, calcium, and membrane potential in wild-type plants subjected to a HL stress treatment applied to a single leaf. *Arabidopsis* plants were untreated or subjected to a high light (HL) stress treatment applied to a single leaf (Local; indicated with a red circle), and ROS **(A)**, calcium **(B)**, or membrane potential **(C)** were imaged, using H_2DCFDA, Fluo-4-AM, or DiBAC$_4$(3), respectively, in whole plants (local and systemic tissues) as described in Fichman and Mittler (2021a), and the Methods section. Scale bar, 1 cm. In support of Figures 1-3. Abbreviations: DiBAC4(3), Bis-(1,3-Dibutylbarbituric Acid)Trimethine Oxonol; H_2DCFDA, 2',7'-dichlorodihydrofluorescein diacetate; HL, high light; ROS, reactive oxygen species; WT, wild-type.

Supplemental Table 1.

List of mutants that were screened for the presence or absence of the systemic ROS wave in response to a local highlight stress applied to a single leaf.

		Accession	Full Name	AGI	ROS wave
	Wild type		*Arabidopsis thaliana* Col-0		+
Receptors					
1.	*crk22-1*	SALK_019124C	cysteine-rich RLK (RECEPTOR-like protein kinase) 22	AT4G23300	+
2.	*crk22-2*	SAIL_765_A07	cysteine-rich RLK (RECEPTOR-like protein kinase) 22	AT4G23300	+
3.	*crk45-1*	SALK_037588C	cysteine-rich RLK (RECEPTOR-like protein kinase) 45	AT4G11890	-
4.	*crk45-2*	SALK_008573	cysteine-rich RLK (RECEPTOR-like protein kinase) 45	AT4G11890	-
5.	*hpca1-1*	DsLoxHs109_07B.0	Hydrogen-peroxide-induced calcium increases 1	AT5G49760	-
6.	*hpca1-2*	SALK_118908C	Hydrogen-peroxide-induced calcium increases 1	AT5G49760	-
7.	*crk2-1*	SK_18638	cysteine-rich RLK (RECEPTOR-like protein kinase) 2	AT1G70520	+
8.	*crk2-2*	SALK_012659C	cysteine-rich RLK (RECEPTOR-like protein kinase) 2	AT1G70520	+
9.	*crk36-1*	SALK_035659C	cysteine-rich RLK (RECEPTOR-like protein kinase) 36	AT4G04490	+
10.	*crk36-2*	SALK_100834C	cysteine-rich RLK (RECEPTOR-like protein kinase) 36	AT4G04490	+
11.	*crk39-1*	SALK_036225C	cysteine-rich RLK (RECEPTOR-like protein kinase) 39	AT4G04540	+
12.	*crk39-2*	SALK_098187C	cysteine-rich RLK (RECEPTOR-like protein kinase) 39	AT4G04540	+

13.	*bak1-1*	SAIL_738_A02	BRI1-associated receptor kinase	AT4G33430	+
14.	*bak1-2*	SALK_034523C	BRI1-associated receptor kinase	AT4G33430	+
15.	*ghr1-1*	SALK_031493C	guard cell hydrogen peroxide resistant 1	AT4G20940	+
16.	*ghr1-2*	SALK_033702C	guard cell hydrogen peroxide resistant 1	AT4G20940	+
17.	*dorn1-1 (p2k1-1)*	EMS mutant	Does not respond to nucleotides 1	AT5G60300	+
18.	*dorn1-3* (*p2k1-3*)	SALK_042209	Does not respond to nucleotides 1	AT5G60300	+

Aquaporins					
19.	*pip1;2-1*	SALK_019794C	Plasma membrane intrinsic protein 1-2	AT2G45960	+ (Fichman et al., 2021a)
20.	*pip1;2-2*	SALK_0145347	Plasma membrane intrinsic protein 1-2	AT2G45960	+ (Fichman et al., 2021a)
21.	*pip1;4-1*	SAIL_75_F07	Plasma membrane intrinsic protein 1-4	AT4G00430	+ (Fichman et al., 2021a)
22.	*pip1;4-2*	SAIL_1166_B06	Plasma membrane intrinsic protein 1-4	AT4G00430	+ (Fichman et al., 2021a)
23.	*pip2;1-1*	*pip2;1-1* (AMAZE collection)	Plasma membrane intrinsic protein 2-1	AT3G53420	- (Fichman et al., 2021a)
24.	*pip2;1-2*	SM_3_35928	Plasma membrane intrinsic protein 2-1	AT3G53420	- (Fichman et al., 2021a)
25.	*pip2;3-1*	SALK_117876	Plasma membrane intrinsic protein 2-3	AT2G37180	+

Kinases					
26.	*cbl4-1*	SALK_113101_16 (CS859749)	Calcineurin b-like protein 4	AT5G24270	-
27.	*cbl4-2*	CS3864	Calcineurin b-like protein 4	AT5G24270	-
28.	*cipk26-2*	SALK_074944C	Calcineurin B-like protein (cbl)-interacting protein kinase 26	AT5G21326	-
29.	*ost1-2*	SALK_020604	Open stomata 1	AT4G33950	-
30.	*ost1-3*	SALK_008068C	Open stomata 1	AT4G33950	-
31.	*ost1-1*	CS161518	Open stomata 1	AT4G33950	-
32.	*kin7-1*	SALK_019840C	Kinase 7	AT3G02880	+ (Fichman et al., 2021a)
33.	*kin7-2*	GT_5_108995	Kinase 7	AT3G02880	+ (Fichman et al., 2021a)
34.	*cbl-pm5*	SALK_110426 X SALK_113101 X SALK_001557 X *cbl8*^{EMS} X SALK_142774	Calcineurin b-like protein 1 Calcineurin b-like protein 4 Calcineurin b-like protein 5 Calcineurin b-like protein 8 Calcineurin b-like protein 9	AT4G17615 AT5G24270 AT4G01420 AT1G64480 AT5G47100	+
35.	*cbl1/9*	SALK_110426 X SALK_142774	Calcineurin b-like protein 1 Calcineurin b-like protein 9	AT4G17615 AT5G47100	-
36.	*cbl1/4/9*	SALK_110426 X SALK_113101 X SALK_142774	Calcineurin b-like protein 1 Calcineurin b-like protein 4 Calcineurin b-like protein 9	AT4G17615 AT5G24270 AT5G47100	-
37.	*cbl1/8/9*	SALK_110426 X *cbl8*^{EMS} X SALK_142774	Calcineurin b-like protein 1 Calcineurin b-like protein 8 Calcineurin b-like protein 9	AT4G17615 AT1G64480 AT5G47100	+

38.	*cbl4/8*	SALK_113101 X *cbl8*^{EMS}	Calcineurin b-like protein 4 Calcineurin b-like protein 8	AT5G24270 AT1G64480	+
39.	*cipk9/23/26*	SALK_058629 X SALK_036154 X GK-703D04	Calcineurin B-like protein (cbl)-interacting protein kinase 9 Calcineurin B-like protein (cbl)-interacting protein kinase 23 Calcineurin B-like protein (cbl)-interacting protein kinase 26	AT1G01140 AT1G30270 AT5G21326	-
40.	*mpk4mpk5*	SALK_056245 X WiscDsLox430A12	Mitogen-activated protein kinase 4 Mitogen-activated protein kinase 5	AT4G01370 AT4G11330	+
41.	*mpk3-1*	SALK_151594	Mitogen-activated protein kinase 3	AT3G45640	+
42.	*mpk4mpk6*	CS69442	Mitogen-activated protein kinase 4 Mitogen-activated protein kinase 6	AT4G01370 AT2G43790	+
43.	*mpk3mpk4*	CS69432	Mitogen-activated protein kinase 3 Mitogen-activated protein kinase 4	AT3G45640 AT4G01370	+
44.	*cpk5-1*	SALK_138808C	calmodulin-domain protein kinase 5	AT4G35310	+
45.	*cpk5-2*	CS65904	calmodulin-domain protein kinase 5	AT4G35310	+
46.	*cpk5-3*	SALK_138912	calmodulin-domain protein kinase 5	AT4G35310	+
47.	*bik1-1*	SALK_005291C	botrytis-induced kinase1	AT2G39660	+
48.	*bik1-2*	SALK_032008	botrytis-induced kinase1	AT2G39660	+
49.	*mkp1-1*	*mkp1-1*	MAP Kinase Phosphatase 1	AT3G55270	-
50.	*mkp1-2*	*mkp1-2*	MAP Kinase Phosphatase 1	AT3G55270	-

Reactive oxygen species					
51.	*rbohD*	CS68747	Respiratory burst oxidase homologue D	AT5G47910	- (Zandalinas et al., 2020b)
52.	*rbohF*	CS68748	Respiratory burst oxidase homologue F	AT1G64060	- (Zandalinas et al., 2020b)
53.	*rbohD/rbohF*	CS68522	Respiratory burst oxidase homologue D Respiratory burst oxidase homologue F	AT5G47910 AT1G64060	- (Zandalinas et al., 2020b)
54.	*gat1*	SALK_078093	GFP arrested trafficking 1	AT2G15570	+ (Fichman et al., 2021a)
55.	*gat1*	SAIL_793_B04.1	GFP arrested trafficking 1	AT2G15570	+ (Fichman et al., 2021a)
56.	*fmo1-1*	SALK_026163	Flavin-dependent monooxygenase 1	AT1G19250	- (Czarnocka et al., 2020)
57.	*lsd1-1*	*lsd1-1*	Lesion simulating disease 1	AT4G20380	+ (Czarnocka et al., 2020)
58.	*lsd1/fmo1*	*lsd1-1* X SALK_026163	Lesion simulating disease 1 Flavin-dependent monooxygenase 1	AT1G19250	+ (Czarnocka et al., 2020)
59.	*apx1*	SALK_000249	Ascorbate peroxidase 1	AT1G07890	+
60.	*apx2*	SALK_091880	Ascorbate peroxidase 2	AT3G09640	+
61.	*apx1/apx2*	SALK_000249 X SALK_091880	Ascorbate peroxidase 1 Ascorbate peroxidase 2	AT1G07890 AT3G09640	+

Calcium					
62.	*glr3.3glr3.6*	SALK_099757 X SALK_091801	Glutamate receptor 3.3 Glutamate receptor 3.6	AT1G42540 AT3G51480	+ (Fichman et al., 2021a)
63.	*glr3.2glr3.6*	SALK_150710 X SALK_091801	Glutamate receptor 3.2 Glutamate receptor 3.6	AT4G35290 AT3G51480	+
64.	*glr3.1glr3.3*	SALK_063873 X SALK_099757	Glutamate receptor 3.1 Glutamate receptor 3.3	AT2G17260 AT1G42540	+
65.	*glr3.1glr3.2*	SALK_063873 X SALK_150710	Glutamate receptor 3.1 Glutamate receptor 3.2	AT2G17260 AT4G35290	+
66.	*glr3.2glr3.3*	SALK_150710 X SALK_099757	Glutamate receptor 3.2 Glutamate receptor 3.3	AT4G35290 AT1G42540	+
67.	*glr3.1glr3.6*	SALK_063873 X SALK_091801	Glutamate receptor 3.1 Glutamate receptor 3.6	AT2G17260 AT3G51480	+
68.	*glr3.3*	SALK_099757	Glutamate receptor 3.3	AT1G42540	+ (Fichman et al., 2021a)
69.	*glr3*.6	SALK_091801	Glutamate receptor 3.6	AT3G51480	+ (Fichman et al., 2021a)
70.	*cngc2-1*	SALK_019922C	Cyclic nucleotide gated channel 2	AT5G15410	- (Fichman et al., 2021a)
71.	*cngc2-2*	SALK_066908C	Cyclic nucleotide gated channel 2	AT5G15410	- (Fichman et al., 2021a)
72.	*msl2-1*	CS69609	Mechanosensitive channels of small conductance–like 2	AT5G10490	- (Fichman et al., 2021a)
73.	*msl2-3*	CS69611	Mechanosensitive channels of small conductance–like 2	AT5G10490	- (Fichman et al., 2021a)
74.	*msl3-1*	CS69719	Mechanosensitive channels of small conductance–like 3	AT1G58200	- (Fichman et al., 2021a)
75.	*msl3-2*	SALK_201695C	Mechanosensitive channels of small conductance–like 3	AT1G58200	- (Fichman et al., 2021a)

76.	*msl10-1*	SALK_076254	Mechanosensitive channels of small conductance–like 10	AT5G12080	+ (Fichman et al., 2021a)
77.	*msl10-2*	SAIL_292_A11	Mechanosensitive channels of small conductance–like 10	AT5G12080	+ (Fichman et al., 2021a)
78.	*msl2/msl3*	CS_69612	Mechanosensitive channels of small conductance–like 2 Mechanosensitive channels of small conductance–like 3	AT5G10490 AT1G58200	-
79.	*msl4/5/6/9/ 10*	CS_69760	Mechanosensitive channels of small conductance–like 4 Mechanosensitive channels of small conductance–like 5 Mechanosensitive channels of small conductance–like 6 Mechanosensitive channels of small conductance–like 9 Mechanosensitive channels of small conductance–like 10	AT1G53470 AT3G14810 AT1G78610 AT5G19520 AT5G12080	+
80.	*mca1-1*	SALK_046108	MID1-complementing activity 1	AT4G35920	+
81.	*mca2-1*	SALK_129208C	MID1-complementing activity 2	AT2G17780	+
82.	*osca1-1*	SALK_038633C	Reduced hyperosmolality-induced Ca^{2+} increase 1	AT4G04340	+ (Fichman et al., 2021a)
83.	*osca1-2*	SAIL_523_G10	Reduced hyperosmolality-induced Ca^{2+} increase 1	AT4G04340	+ (Fichman et al., 2021a)
84.	*tpc1-1*	SALK_074094	Two-pore channel 1	AT4G03560	+ (Fichman et al., 2021a)
85.	*tpc1-2*	SALK_125650	Two-pore channel 1	AT4G03560	+ (Fichman et al., 2021a)

86.	*ann1-1*	SALK_015426C	Annexin 1	AT1G35720	+ (Fichman et al., 2021a)
87.	*ann1-2*	GABI_327B12	Annexin 1	AT1G35720	+ (Fichman et al., 2021a)
88.	*cnx1-1*	SAIL_211_D10	calnexin 1	AT5G61790	+
89.	*cnx1-2*	SALK_083600C	calnexin 1	AT5G61790	+
90.	*crt1-1*	SALK_142821C	calreticulin 1	AT1G56340	+
91.	*crt1-2*	SALK_137641C	calreticulin 1	AT1G56340	+
92.	*aca4-1*	SALK_029620	autoinhibited Ca(2+)-ATPase, isoform 4	AT2G41560	+
93.	*aca8-1*	SALK_057877	autoinhibited Ca2+ -ATPase, isoform 8	AT5G57110	+
94.	*aca8-2*	SALK_108260	autoinhibited Ca2+ -ATPase, isoform 8	AT5G57110	+
95.	*aca11-1*	SAIL_269_C07	autoinhibited Ca2+-ATPase 11	AT3G57330	+

Plasmodesmata-trafficking					
96.	*pdlp1-1*	SAIL_515_B10	plasmodesmata-located protein 1	AT5G43980	- (Fichman et al., 2021a)
97.	*pdlp1-2*	SM_3_36596	plasmodesmata-located protein 1	AT5G43980	- (Fichman et al., 2021a)
98.	*pdlp5-1*	SALK_044770	plasmodesmata-located protein 5	AT1G70690	- (Fichman et al., 2021a)
99.	*pdlp5-2*	SAIL_46_E06	plasmodesmata-located protein 5	AT1G70690	- (Fichman et al., 2021a)
100.	*cher1-1*	SALK_065853	choline transporter-like 1	AT3G15380	+
101.	*cher1-2*	SALK_056391	choline transporter-like 1	AT3G15380	+

G-proteins					
102.	*agb1-2*	CS6536	GTP binding protein beta 1	AT4G34460	+
103.	*αβagg123*	gpa1-1 X agb1-1 X CS16551 X CS807967	G protein alpha subunit 1 GTP binding protein beta 1 Arabidopsis G protein gamma subunit 1 Arabidopsis G protein gamma subunit 2 Arabidopsis G protein gamma subunit 3	AT2G26300 AT4G34460 AT3G63420 AT3G22942 AT5G20635	+
104.	*agg3*	CS807967	Arabidopsis G protein gamma subunit 3	AT5G20635	+
105.	*agg123*	CS16551 X CS807967	Arabidopsis G protein gamma subunit 1 Arabidopsis G protein gamma subunit 2 Arabidopsis G protein gamma subunit 3	AT3G63420 AT3G22942 AT5G20635	+
106.	*αβxlg123*	gpa1-1 X agb1-1 X CS873748 X SALK_062645 X CS806006	G protein alpha subunit 1 GTP binding protein beta 1 Extra-large G protein 1 Extra-large G protein 2 Extra-large G protein 3	AT2G26300 AT4G34460 AT2G23460 AT4G34390 AT1G31930	+
107.	*xlg123*	CS873748 X SALK_062645 X CS806006	Extra-large G protein 1 Extra-large G protein 2 Extra-large G protein 3	AT2G23460 AT4G34390 AT1G31930	+

Transcription factors					
108.	*myb30-1*	SALK_122884	MYB domain protein 30	AT3G28910	+ (Fichman et al., 2020)
109.	*myb30-2*	SALK_027644	MYB domain protein 30	AT3G28910	+ (Fichman et al., 2020)
110.	*wrky48-1*	SALK_066438C	WRKY DNA-binding protein 48	AT5G49520	+
111.	*wrky48-2*	SALK_144719C	WRKY DNA-binding protein 48	AT5G49520	+
112.	*gata8-1*	SALK_091040C	GATA transcription factor 8	AT3G54810	+ (Fichman et al., 2020)
113.	*gata8-2*	SALK_148073C	GATA transcription factor 8	AT3G54810	+ (Fichman et al., 2020)

Others					
114.	*aos-1*	SALK_017756C	Allene oxide synthase	AT5G42650	+ (Zandalinas et al., 2020a)
115.	*gdsl-1*	SALK_005724C	GDSL esterase/Lipase	AT1G29670	+ (Fichman et al., 2020)
116.	*gdsl-2*	SALK_025240C	GDSL esterase/Lipase	AT1G29670	+ (Fichman et al., 2020)
117.	*opr1-1*	SALK_145353	12-oxophytodienoate reductase 1	AT1G76680	+
118.	*opr1-2*	SALK_021313C	12-oxophytodienoate reductase 1	AT1G76680	+
119.	*gun1-102*	SAIL_290_D09	Genomes uncoupled 1	AT2G31400	+
120.	*gun5-1*	EMS	Genomes uncoupled 5	AT5G13630	+

Photoreceptors					
121.	*phyA*	phyA-211	Phytochrome A	AT1G09570	+ (Devireddy et al., 2020)
122.	*phyB*	SALK_069700C	Phytochrome B	AT2G18790	- (Devireddy et al., 2020)
123.	*phyB-9*	phyB-9	Phytochrome B	AT2G18790	- (Fichman et al., 2021b)
124.	*phyA/ phyB*	phyA-201 X phyB-8-36	Phytochrome A Phytochrome B	AT1G09570 AT2G18790	- (Devireddy et al., 2020)

Acknowledgment

We thank The Arabidopsis Biological Resource Center (ABRC), and Professors E.E. Farmer, S. Karpinski, E. Liscum, C. Maurel, S. Pandey, A. S. Richter, G. Stacey and S. Zhang for the seeds that were used for this screen.

References

Czarnocka, W., Fichman, Y., Bernacki, M., Różańska, E., Sańko-Sawczenko, I., Mittler, R., and Karpiński, S. (2020). FMO1 is involved in excess light stress-induced signal transduction and cell death signaling. Cells **9**:2163.

Devireddy, A. R., Liscum, E., and Mittler, R. (2020). Phytochrome B is required for systemic stomatal responses and reactive oxygen species signaling during light stress. Plant Physiol. **184**:1563–1572.

Fichman, Y., Zandalinas, S. I., Sengupta, S., Burks, D., Myers, R. J., Azad, R. K., and Mittler, R. (2020). MYB30 orchestrates systemic reactive oxygen signaling and plant acclimation. Plant Physiol **184**:666–675.

Fichman, Y., Myers, R. J., Grant, D. G., and Mittler, R. (2021a). Plasmodesmata-localized proteins and ROS orchestrate light-induced rapid systemic signaling in Arabidopsis. Sci. Signal. **14**:eabf0322.

Fichman, Y., Xiong, H., Sengupta, S., Azad, R. K., Hibberd, J. M., Liscum, E., and Mittler, R. (2021b). Phytochrome B regulates reactive oxygen signaling during abiotic and biotic stress in plants. BioRxiv doi:10.1101/2021.11.29.470478.

Zandalinas, S. I., Fichman, Y., Devireddy, A. R., Sengupta, S., Azad, R. K., and Mittler, R. (2020a). Systemic signaling during abiotic stress combination in plants. Proc. Natl. Acad. Sci. U.S.A. **117**:13810–13820.

Zandalinas, S. I., Fichman, Y., and Mittler, R. (2020b). Vascular bundles mediate systemic reactive oxygen signaling during light stress. Plant Cell **32**:3425–3435.